



POLITECNICO DI TORINO

Department of Environment, Land and Infrastructure Engineering

Master of Science in Petroleum Engineering

Processing Workflow for Estimation of Dispersion Curves from Seismic Data and QC

Supervisor:

Prof. Laura Valentina Socco

Student:

Mohammadkarim Karimpour

OCTOBER 2018

Thesis submitted in compliance with the requirements for the Master of Science degree

Acknowledgments

I would like to thank all the people who supported me in this way, people who shared their time and valuable ideas.

First of all, I would like to thank my supervisor for her continuous guiding and advising me during these past months, thank you to Laura Valentina Socco for her approach to teaching which inspired me to do this thesis. She has been a precious source of ideas to me and her extreme patience to review and correct this work played a significant role to advance this thesis.

Thanks to Farbod Khosro Anjom, for his continuous contribution to clarify my doubts, and his precious guidance about the used codes.

And thanks to my family for their unconditional support.

Thanks to people at Total E & P for allowing me to use their dataset
and publish the results.

Table of Contents

Acknowledgments	2
List of Figures	vi
Introduction.....	ix
Chapter I. Overview of the Surface Wave Method	12
1.1 Rayleigh Wave Propagation	12
1.2 Surface Wave Analysis	15
1.3 Surface Wave Propagation in a Laterally Heterogeneous Environment	16
1.4 Spatial Windowing	18
Chapter 2 Method	20
2.1. Dividing Receivers Line into Segments	20
2.2 Gaussian Windowing	22
2.2.1 Resolution Issues	25
2.3 Overlap of Adjacent Line Segments	27
2.4 Quality Control	28
2.4.1 Experimental uncertainty based on sources on each side	28
2.4.2 Experimental uncertainty based on all shots	31
2.4.3 Frequency bandwidth	32
Chapter 3 Data, Processing and Results	34

3.1	Data	34
3.2	Processing.....	35
3.3	Results	38
	3.3.1 Determination of Maximum Allowable Source-Receiver Distance	38
	3.3.2 Determination of Minimum Acceptable Offset	41
	3.3.3 Segment Size L	42
	3.3.4 Determination of Alpha and Beta	43
	3.3.5 Overlap of Adjacent Segments.....	46
	3.3.6 Final Design for Dispersion Curve Extraction	46
	3.3.7 Retrieved Dispersion Curves.....	47
3.4	Quality Control Results	51
	3.4.1 Experimental Uncertainty based on Sources on each side.....	51
	3.4.2 Experimental Uncertainty based on all Shots.....	59
	3.4.3 Experimental Uncertainty based Frequency Bandwidth	61
	3.4.4 Cross-plots of Uncertainty Indices.....	62
	Conclusions	67
	References	69

List of Figures

Figure 1.1. <i>Wave velocities in different environments</i>	13
Figure 1.2. <i>Example of modal curves</i>	14
Figure1.3. <i>Three main steps of surface wave method</i>	16
Figure2.1. <i>Scheme of maximum acceptable offset</i>	21
Figure 2.2. <i>Scheme of receiver segment and shots</i>	21
Figure 2.4. <i>Effect of α on Gaussian window shape</i>	24
Figure 2.5. <i>Effect of Gaussian window shape on lateral resolution</i>	25
Figure 2.5. <i>Effect of receiver segment size on wavenumber and lateral resolution</i>	26
Figure 2.6. <i>Scheme of adjacent segments overlap</i>	28
Figure 2.7. <i>Schematic example of misfit between dispersion curves retrieved from negative and positive offsets</i>	29
Figure 2.8. <i>Schematic example of experimental uncertainties in dispersion curves</i>	32
Figure 3.1. <i>Schematic picture of the location where the dataset was gathered</i>	34
Figure 3.2. <i>The f-k spectrum of the window centered on 339th receiver</i>	36
Figure 3.3. <i>The f-k spectra alongside the DC of the Gaussian window with maximum locating on the 339th receiver</i>	37
Figure 3.4. <i>Dispersion curves of the Gaussian window centered on the 140th receiver</i>	39
Figure 3.6. <i>Scheme of maximum offset test</i>	41
Figure 3.7. <i>Minimum offset determination based on the dispersion curves</i>	42
Figure 3.8. <i>Example of wavenumber resolution determination</i>	44

Figure 3.9. <i>Lateral resolution and f-k spectra resolution in case of 15 receivers.</i>	45
Figure 3.10. <i>Pseudo-section corresponding to total offsets.</i>	48
Figure 3.11. <i>All the retrieved dispersion curves related to total shots along seismic line.</i>	49
Figure 3.12. <i>All of the obtained dispersion curves from positive offsets along seismic line.</i>	50
Figure 3.13. <i>All the dispersion curves obtained from left shots along seismic line.</i>	51
Figure 3.14. <i>Dispersion Curve of the Gaussian window with maxima located on 134th receiver.</i>	52
Figure 3.15. <i>Dispersion curve of the Gaussian window centered on the 200th receiver.</i> ..	53
Figure 3.16. <i>The retrieved DC of the Gaussian window centered on the 525th receiver.</i> ..	54
Figure 3.17. <i>An example for low phase velocity deviation which occurs at 423rd receiver.</i>	55
Figure 3.19. <i>Average phase velocity deviation along the seismic line.</i>	57
Figure 3.20. <i>Division of survey line into low, medium and high quality categories.</i>	58
Figure 3.21. <i>Distribution of the average phase velocity deviation along the seismic line.</i>	59
Figure 3.22. <i>Experimental Uncertainties as a function of window maxima location.</i>	60
Figure 3.22. <i>Minimum frequency, maximum frequency and frequency band of total offsets along the seismic line.</i>	61
Figure 3.23. <i>Frequency band as a function of receiver number.</i>	62
Figure 3.24. <i>Cross-plot of experimental uncertainties based on all shots and frequency bandwidths.</i>	63

Figure 3.25. <i>Cross-plot of phase velocity deviations and frequency bands.</i>	64
Figure 3.25. <i>Cross-plot of uncertainties of shots on each side and phase velocity deviations.</i>	65
Figure 3.26. <i>Cross-plot of the three uncertainty indices.</i>	66

Introduction

In hydrocarbon exploration, the exploration operation mainly consists of interpretation of seismic reflection waves. Surface waves significantly affect the deep imaging results since they can mask the reflection data. So, it is necessary to remove surface waves, called also ground roll, from seismograms in deep explorations to increase the accuracy of the acquired data. This is not an easy task since the ground roll is considered as coherent noise. Some of the suggested methods to reduce the negative effect of ground roll, can also contribute to near-surface characterization. They include analyzing the results in $f-k$ domain (Nolet and Panza, 1976; Tselentis and Delis, 1998) or in $\omega-p$ domain (McMechan and Yedlin, 1981).

Near-surface characterization is of paramount importance since its results can be used in static corrections which is an important step in data processing. This, in turn, leads to more precise subsurface model particularly in deep hydrocarbon explorations.

Surface-wave methods (SWMs) are seismic characterization methods which have been used to retrieve S-wave velocity models. SWMs use the geometric dispersion as the physical principle to measure the dispersive features of a site and calculate the subsoil characteristics. SWMs consist of three main steps: acquisition, processing and inversion.

In the present work, we have focused on data processing step. Since we are given dataset which reflects a 12 km seismic line, we need to divide this line into different segments to be able to process the data. The final goal of data processing is to extract several dispersion curves which are used later as inputs in inversion. We have included

lateral variations in our data processing by using Gaussian windowing technique (Bergamo et al., 2012).

Gaussian windowing is a spatial windowing technique which is particularly useful in case laterally heterogeneous environments. This method extracts DCs which reflect local properties of subsoil.

The following chapters of this work mainly focus on 2 issues:

- Optimization of parameters of Gaussian moving window in order to process the data in a laterally variable environment using field data.
- Analyzing the extracted dispersion curves along the survey line in order to assess the quality of our results. We implement quality control to evaluate the degree of uncertainty in the obtained dispersion curves.

So, we expect to achieve the second target of this work, by comparing the retrieved dispersion curves for each window along the seismic line and based on this comparison, subsoil can be divided into three quality classes. This classification gives us quick estimations about the dispersion curves that can be used for inversion.

In the first chapter, basics of surface wave methods are discussed. Then, the general formulas for surface wave propagation in a laterally heterogeneous environment are presented.

The second chapter describes the processing methodology applied in this work to extract the dispersion curves, the method is based on Gaussian windowing of the

seismic records. We discuss about its theory and relevant equations and the applied procedure to obtain the results.

In the third chapter, we describe the data used in the present work. Then, the results of our work will be presented. The relevant outputs of the applied methods are brought together. Several analysis on the results are performed including interpretation of the dispersion curves. Afterwards, the quality control indices are applied to the extracted dispersion curves to investigate their quality.

Chapter I.

Overview of the Surface Wave Method

The surface wave method (SWM) is a seismic characterization method based on the analysis of the geometric dispersion of surface waves. The dispersion characteristics are estimated from seismic record and then inverted in order to retrieve the vertical profile of shear wave velocity. Different dispersion waves like Rayleigh waves, Scholte, Love and P-guided can be analyzed. However, the most widely used approach refers to Rayleigh waves.

1.1 Rayleigh Wave Propagation

Rayleigh waves propagate parallel to the Earth's surface without spreading energy toward the Earth's interior. Their amplitude decreases with depth and majority of the energy propagates until a depth almost equal to one wavelength. A propagating Rayleigh wave contains different harmonics with different wavelengths which propagate with different penetration depths. In a homogenous medium, all the wavelengths have the same phase velocity because the seismic properties are the same for all of them. However, in a vertically heterogeneous environment different wavelengths travel through different media, so the different frequencies have different propagation velocities (figure 1.1). In a vertically heterogeneous medium, Rayleigh waves propagation is dispersive which means different frequencies have different phase velocities. Geometric dispersion which depends

on the geometry of the investigated subsoil, is used to extract information about the subsurface media.

As a result, dispersion curve is defined as the relation between frequency and phase velocity. At high frequencies (short wavelengths) the phase velocity corresponds to the shallower layers, and the effect of deeper layers can be seen at low frequencies (long wavelengths).

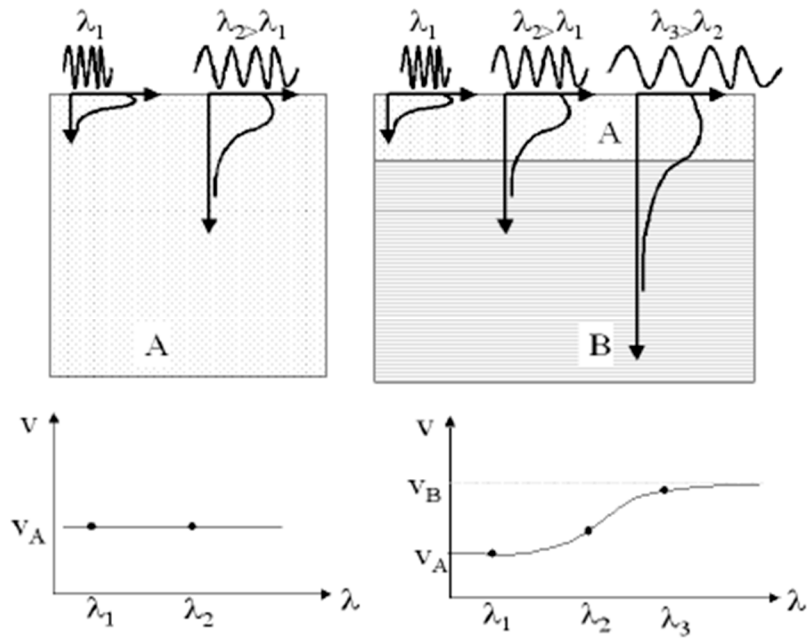


Figure 1.1. *Wave velocities in different environments. In a homogenous environment (left) the velocity is constant for all wavelengths while in a vertically heterogeneous media (right) phase velocity is a function of wavelength (Strobbia 2003).*

As a matter of fact, surface waves propagation in a layered media is a multi-modal phenomenon, it means at each frequency different phase velocities can exist at the same time, each phase velocity corresponds to a different mode of propagation (figure 1.2).

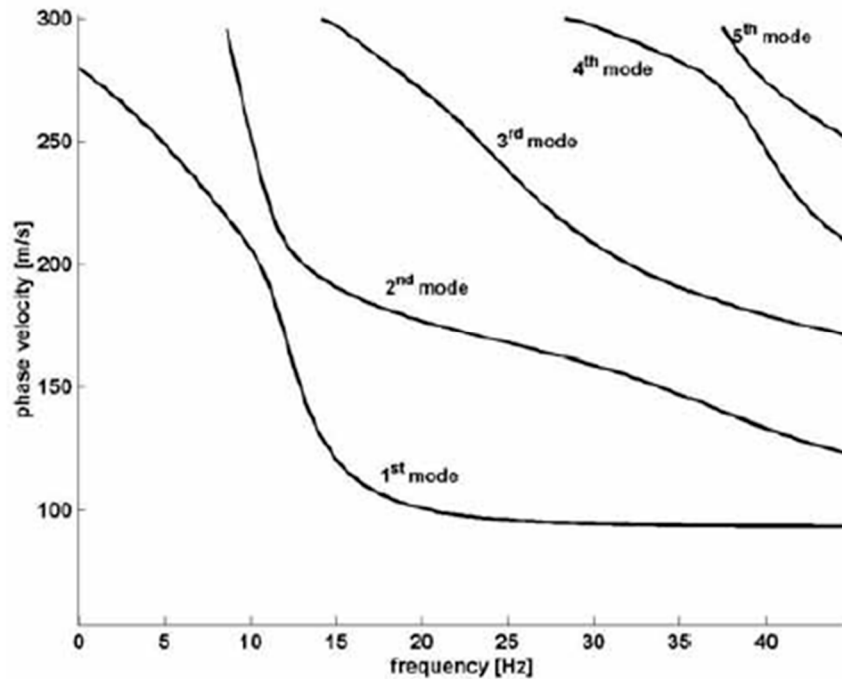


Figure 1.2. Example of modal curves (Socco and Strobbia, 2004).

The mode with lowest frequency is called fundamental mode. Although the fundamental mode is often the dominant one, higher modes have significant importance in many cases and they cannot be ignored. When the velocity of different modes is so close to one another, separation of modal curves can be very difficult, so in this situation modal curves superimpose to one another in frequency domain.

As a result of modal superposition, the generated phase velocities at this situation are only apparent velocities, and the corresponding DC is an apparent dispersion curve.

Due to complexity of apparent dispersion curve modeling and the role of unknown parameters (like material damping and source characteristics), only the fundamental mode is used in most of the processing methods.

1.2 Surface Wave Analysis

Valuable information can be retrieved by analysis of Rayleigh wave dispersion.

The surface wave method consists of three main steps:

1. Acquisition
2. Processing
3. Inversion

The acquisition step includes gathering seismic data including surface waves in a wide frequency band. The processing deals with extraction of dispersion curves from seismic records. Finally, model parameters are estimated through inversion procedure (figure 1.3).

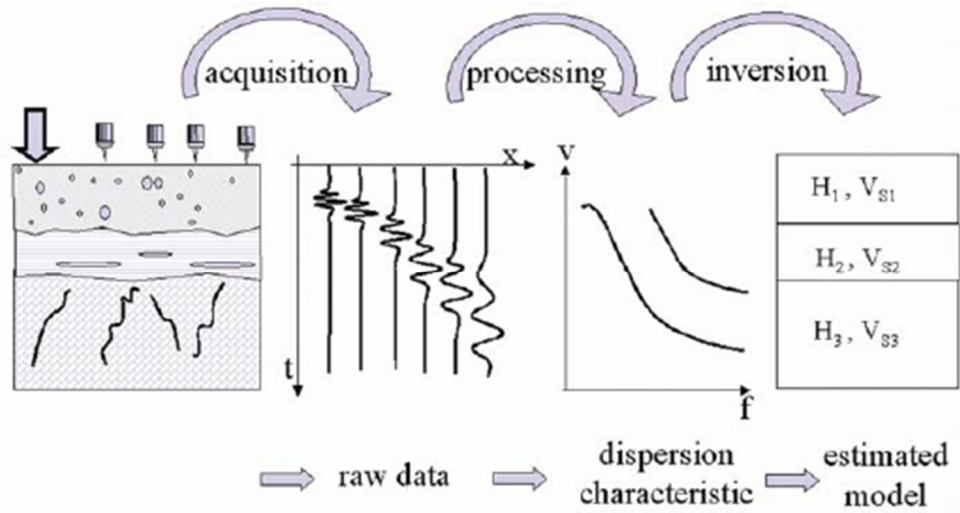


Figure 1.3. Three main steps of surface wave method (Strobbia, 2003).

In the following parts of this work, we focus on processing step of surface wave method.

1.3 Surface Wave Propagation in a Laterally Heterogeneous Environment

The path-average approximation can be used in order to check if 1D surface wave method is applicable in presence of lateral variations. This can be achieved by the analysis performed by Woodhouse (1974) for surface wave traveling in a quasi-stratified media with slowly varying seismic properties.

The dispersion characteristics of subsoil beneath the point of interest determine the local phase velocity of each mode (Yanovskaya, 2002). So, the integral of the local phase slowness p is equal to the total phase-lag along a path. For the i^{th} mode we have:

$$\omega \phi_j(\omega) = \omega \int_{ray_j} p_j(x, \omega) dx \quad (1.1)$$

Where ω is angular frequency, $p_j(x, \omega)$ is slowness distribution along the ray path and $\phi_j(\omega)$ is the total phase-lag along the ray path for the j^{th} mode. Representation of the phase in this way has some limitations for the vector harmonics in stratified case. To overcome this issue, we need for a propagation range X and S-wave velocity β , the combination $\omega\beta^{-1}X \gg 1$. It means that the path-average approximation breaks down in presence of rapid variations of seismic properties in comparison to wavelengths of the surface waves. In such a strong heterogeneous environment it is so probable to observe modal coupling, and considerable deviations of surface wave path from the shortest way between source and receiver. Marquering et al. (1996) showed that in case of weak variations of seismic parameters of subsoil, the formulation for a stratified medium can be adopted.

Moreover, we can simplify propagation component if it is not far from the shortest path by applying the structure that generates the same incremental phase. Therefore, we can obtain the average slowness $\langle p_j(\omega) \rangle$ of the j^{th} mode as:

$$\phi_j(\omega) = X \langle p_j(\omega) \rangle \quad (1.2)$$

Where X is the distance between source and receiver known as offset. When the ray path deviates from the shortest source-receiver distance, $p_j(\omega)$ is overestimated since the true path length is more than the offset X .

In case of a stratified structure, we can write for a number of modes the contribution to the surface wave part of the seismogram as:

$$u(X, \omega) = \sum_{j=0}^J R_j(X, \omega) \exp \left(-i \omega \int_{xy_j} dx (p_j(x, \omega)) \right) S_j(\omega) \quad (1.3)$$

Where $R_j(X, \omega)$ contains terms which depend on receiver depth and geometric spreading of the surface waves and $S_j(\omega)$ is representative of the imposed excitation by the source. Surface wave attenuation can be included by considering local phase slowness p_j to be complex. Kennett (1995) stated that contributions of R_j and S_j are not localized in a laterally varying structure even if they are evaluated using the models appropriate to the source and receiver locations.

Moreover, it has been proved that applying 1D approach in 2D environments, can produce unsatisfactory and even misleading results (Boiero and Socco, 2011).

1.4 Spatial Windowing

When the lateral variability in the medium is not weak, the estimated dispersion curve is not representative of average slowness. To overcome this issue, dispersion curve should become a local property of the investigated portion of subsoil. Spatial windowing is the applicable tool to achieve this aim. There are different types of spatial windowing such as box, Hanning and Gaussian windowing. We have chosen Gaussian windowing in our work since the use of Gaussian windowing enables us to extract several local dispersion curves from a single seismic record. Moreover, the Gaussian window is a good balance between high wavenumber resolution of the Hanning window and high lateral resolution

of the box window. Further explanations of Gaussian windowing technique are stated in the next chapter.

2.1. Dividing Receivers Line into Segments

It is necessary to divide receiver line into different segments particularly if the survey line covers considerable distances. A seismic line usually consists of several receivers and shots. If the distance between a source and receiver increases significantly, the signal to noise ration becomes unacceptable. So, we should find the maximum offset which satisfies the desired signal to noise ratio. Figure 2.1 displays the maximum acceptable offset schematically.

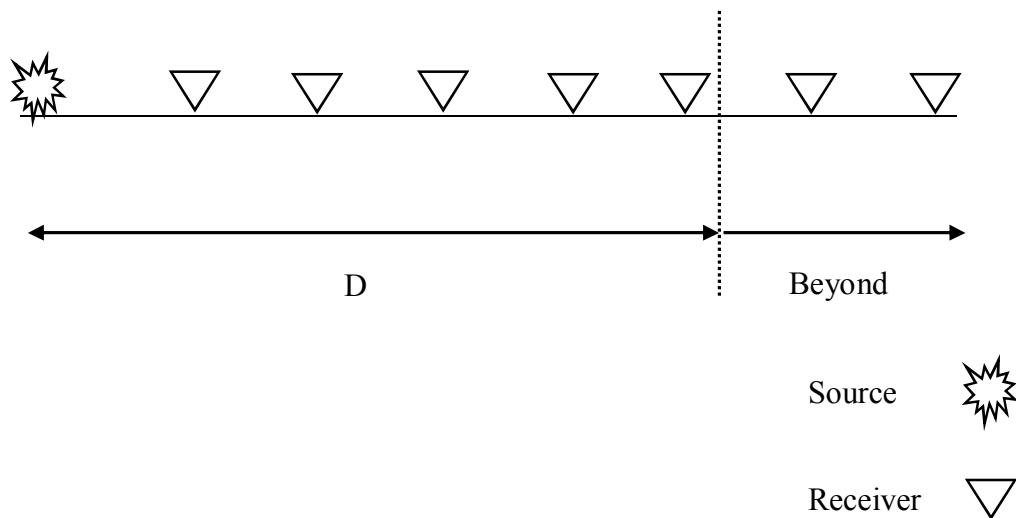


Figure 2.1. *Scheme of maximum acceptable offset. D is the maximum acceptable offset.*

After determination of maximum offset, this distance should be shared between receiver segment and number of shots since higher number of shots leads to higher signal to noise ratio. We can see schematically the division of D between receiver segment and sources in figure 2.2.

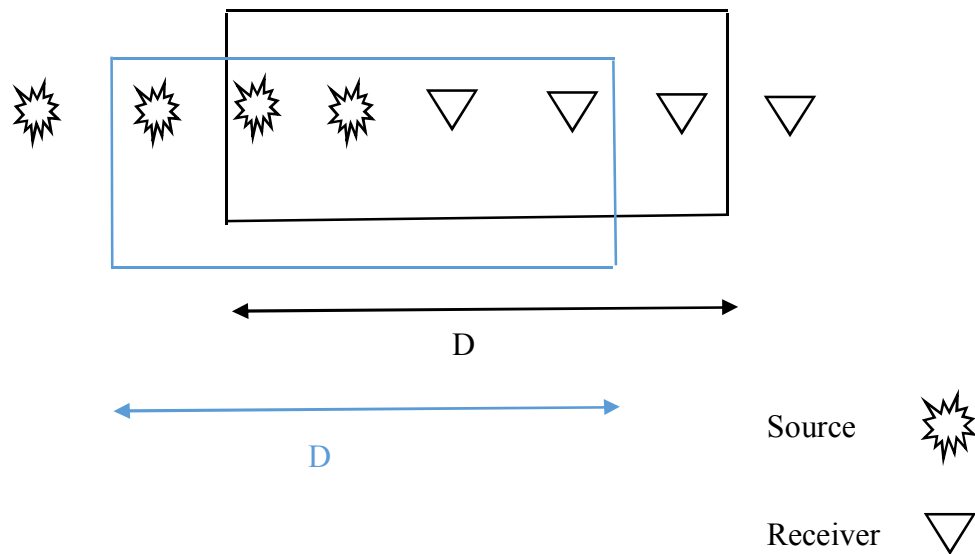


Figure 2.2. *Scheme of receiver segment and shots.*

As it is shown in figure 2.2, there are different options for division of D between shots and receiver segment. Choosing higher number of receivers leads to lower number of shots and vice versa. Therefore, there should be a balance between length of receiver

segment and number of shots. It should be noticed that shots exist also at the right side of receivers but in order to avoid complexity in figure 2.2, only shots at the left side of the receivers have been shown.

2.2 Gaussian Windowing

As mentioned earlier, presence of lateral variation below the survey line makes the dispersion curves of a 1D approach to be unrepresentative of subsoil characteristics because 1D method neglects lateral heterogeneities. One method to overcome this issue is to use spatial windowing which makes the dispersion curve representative of the local velocity of the subsoil beneath the window maxima.

In spatial windowing of the seismic traces, each trace amplitude is differently weighted. This in turn, makes the dispersion curve a local property of the subsurface parts with are weighted more. Bohlen (2004) suggested to apply a moving spatial window to extract dispersion curves and using them to generate a 2D shear wave velocity pseudo-section as a result of inversion process. Bergamo et al. (2012) proposed a technique using space-varying spatial windowing to retrieve 2D structures from surface wave data. They used Gaussian moving windows to obtain dispersion curves which represent local properties of the subsurface. Each dispersion curve represents a different portion of the investigated subsoil (figure 2.3). If more than one shot is available for the same array, signal-to-noise ratio can be improved by stacking process in f-k spectra (Neduzca, 2007). Then, to obtain dispersion curves with higher qualities, picking of maxima is performed on each stacked f-k spectra.

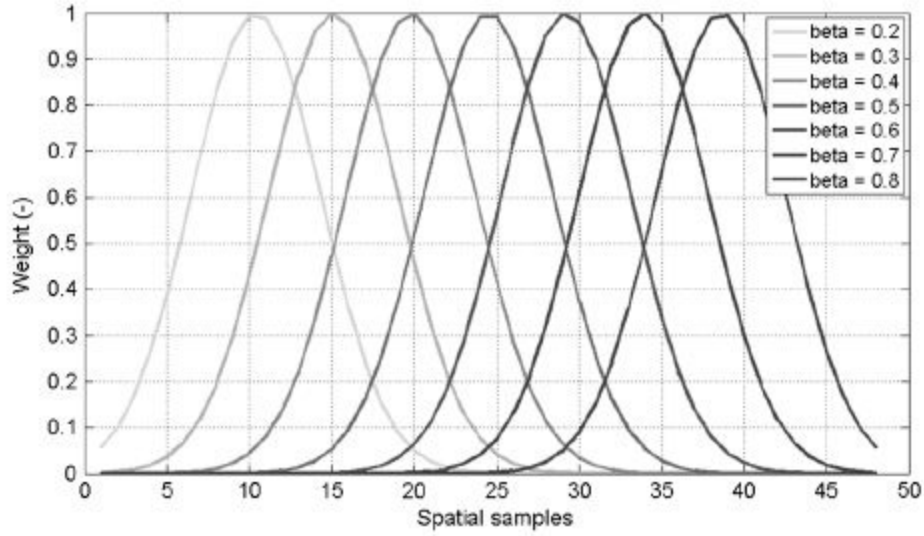


Figure 2.3. Gaussian window spans the whole array interval. (Bergamo et al., 2012) The plot shows how a Gaussian window covers the whole array length through varying number of beta. Beta reflects relative position of the window maximum with respect to the array length.

The Gaussian window is defined as follows:

$$w_{k+1} = \exp\left(-\frac{1}{2}\left(\alpha \frac{k - N\beta}{N/2}\right)^2\right) \quad (2.1)$$

And $k = 0, 1, \dots, N$

Where w is the assigned weight to the $k+1$ th trace, N is the number of spatial samples minus one, β identifies the location of the maximum of the window and α shows the width of windows.

There are two parameters affecting the shape of the window in Gaussian windowing process. Parameter α identifies the width of the window. In other words, it controls the investigated portion of subsurface by each window. The minimum value for α is 2 and it

is inversely proportional to the window standard deviation according to the following equation:

$$\sigma = \frac{N}{2\alpha} \quad (2.2)$$

According to equation 2.2, α determines the value for σ . Therefore, it specifies the lateral resolution of dispersion curves. Figure 2.4 shows the impact of α on the shape of the window.

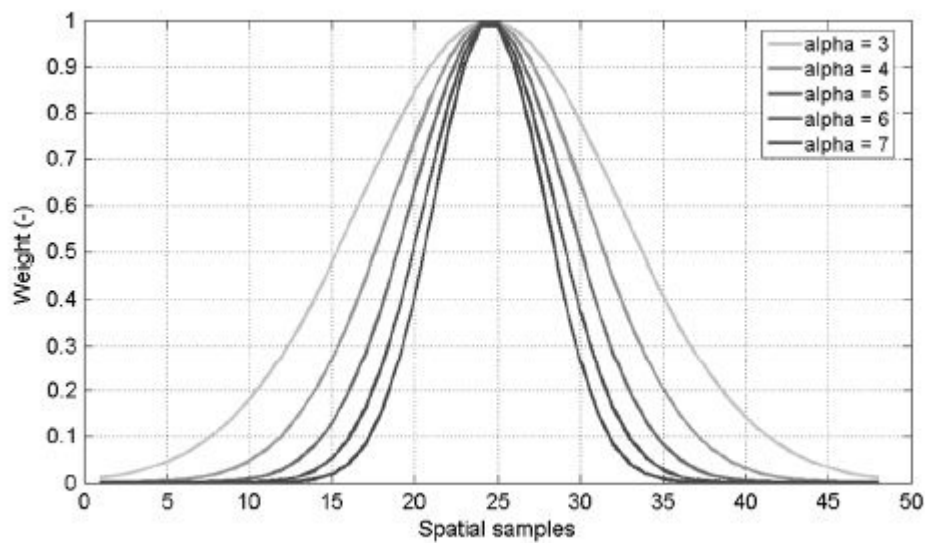


Figure 2.4. *Effect of α on Gaussian window shape (Bergamo et al., 2012).*

Higher values of α lead to less window width. β is 0.5 for all windows.

The other important parameter affecting window shape is β . Its range is from zero to one which specifies the position of the window maximum with respect to the array length. Figure 2.1 displays the window maximum location for different values of β .

2.2.1 Resolution Issues

Using the spatial windowing has some consequences on the wavenumber resolution of f-k spectra and lateral resolution of the dispersion curves. Lateral resolution of a dispersion curve is defined as the portion of subsurface which the dispersion curve is representative of. This width has been conventionally considered as 2σ (Bergamo et al. 2012). It means every single retrieved dispersion curve displays seismic properties of a subsurface portion which is centered at the Gaussian window maximum and σ wide on both sides (figure 2.5).

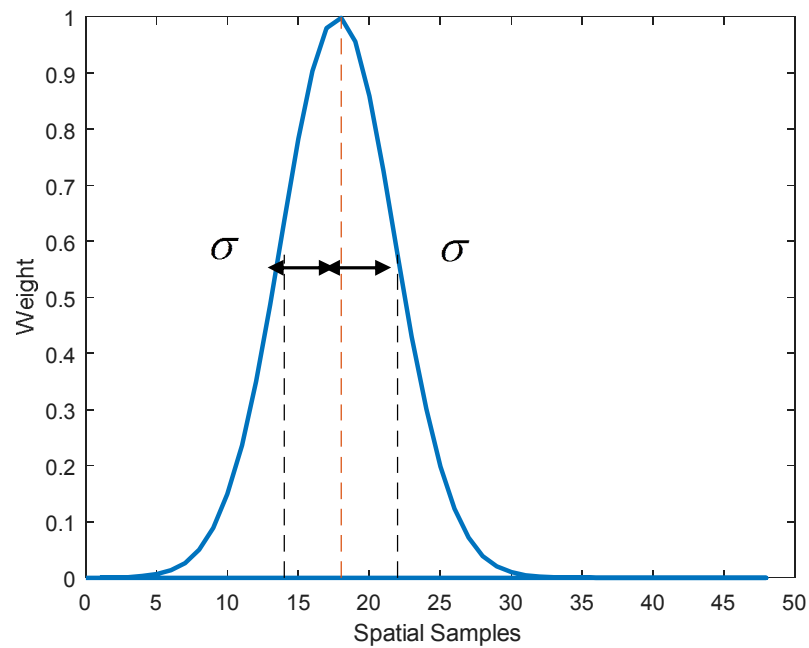


Figure 2.5. *Effect of Gaussian window shape on lateral resolution. Here, α is 6 and β is equal to 0.35.*

According to equation 2.2 and figure 2.5, choosing a large value of α leads to small value of standard deviation σ , which improves the lateral resolution. However, as mentioned earlier, α should be selected small enough to guarantee the needed wavenumber resolution of the f-k spectra.

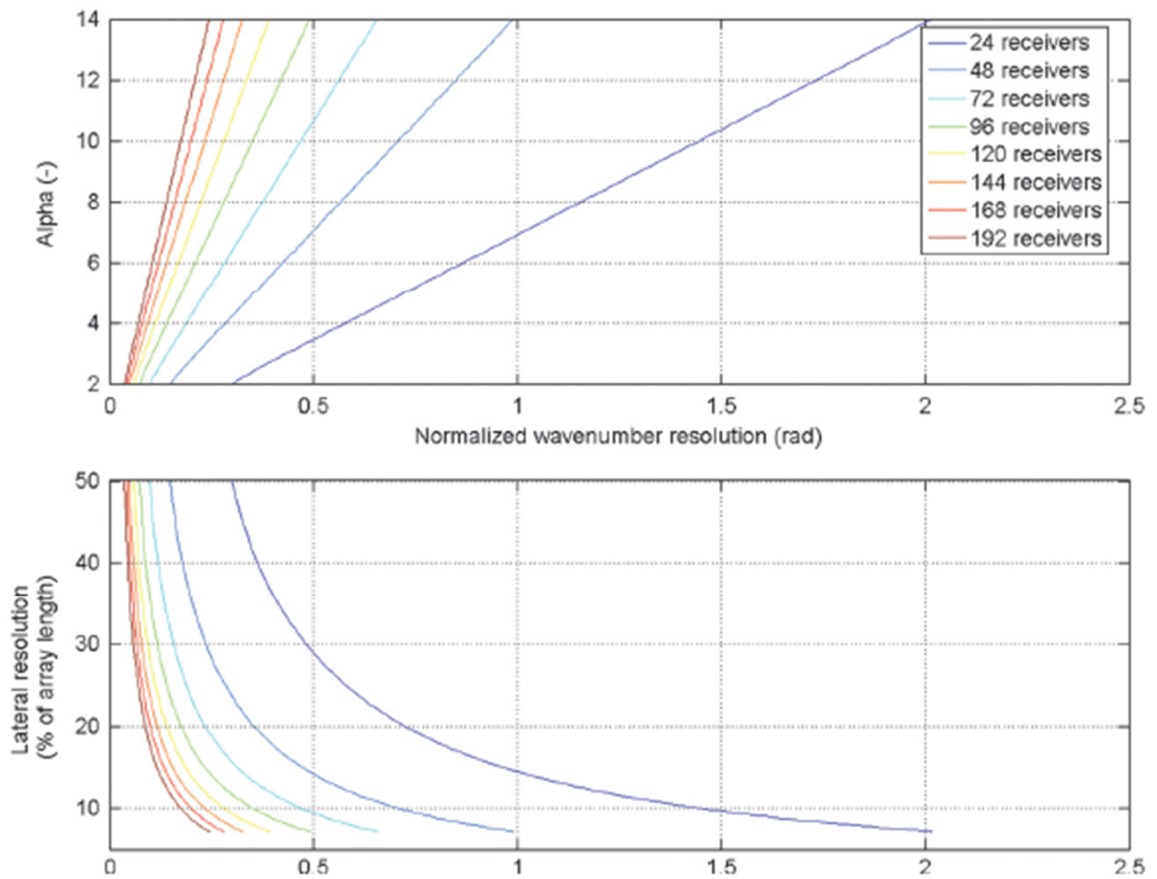


Figure 2.5. *Effect of receiver segment size on wavenumber and lateral resolution (Bergamo et al., 2012). The plot displays the relationship among receiver segment, value of α , lateral resolution and spectral resolution for several array configurations.*

It can be seen that for the same value of α , increasing number of receivers in receiver segment leads to higher spectral resolution, however, the corresponding lateral resolution decreases.

Having the wavenumber resolution, the relevant value for α is obtained through the first part of figure 2.5. Then, having known the value of α , we get the guaranteed value for the corresponding lateral resolution through the second part of figure 2.5.

2.3 Overlap of Adjacent Line Segments

Adjacent line segments need to have a certain overlap in order to retrieve dispersion curves representative of the whole survey line. As a matter of fact, the information at edges of each interval can be lost if the considered overlap is not sufficient. Positions of Gaussian window centers in two different segments are shown schematically in figure 2.6. It can be seen that if there is no overlap between these two segments, we will observe a gap between the position of last Gaussian window in the first segment and the location of first window in the second segment.

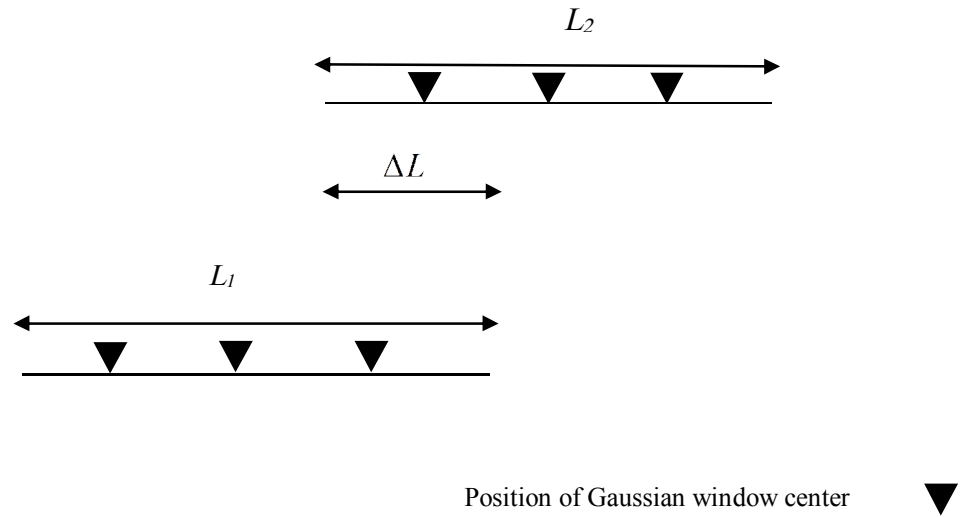


Figure 2.6. Scheme of adjacent segments overlap. L_1 and L_2 display the receivers segment size and ΔL shows the amount of adjacent segments overlap.

2.4 Quality Control

In this part, we check the quality of our extracted dispersion curves. It can be done by using different indices which will be explained in this section. In general, uncertainties in dispersion curves originate from different reasons such as random noise while data acquisition and lateral variations. Here, we consider lateral variations as the main cause of uncertainties in the extracted dispersion curves.

2.4.1 Experimental uncertainty based on sources on each side

The media beneath the receivers is not 1D and we will see difference in propagation patterns according to the propagation direction. Therefore, if we use shots at the two sides of the segment, we will obtain different dispersion curves when there are significant lateral variations. These curves do not exactly match each other and exhibit misfit which varies along the survey line. An example of misfit between dispersion curves is displayed schematically in figure 2.7.

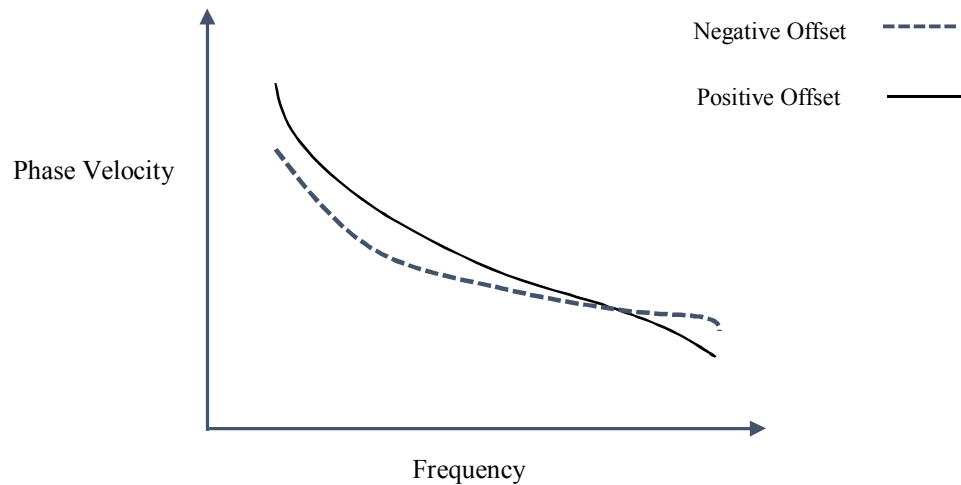


Figure 2.7. *Schematic example of misfit between dispersion curves retrieved from negative and positive offsets.*

Here, our idea is to relate the misfit between the dispersion curves obtained from positive and negative offsets of each Gaussian window, to lateral variations at that portion of subsurface

So, for every pair of dispersion curves (retrieved from positive and negative offsets) along the seismic line, the average phase velocity at each frequency is calculated simply by using arithmetic average method. We use average velocities to calculate phase velocity deviations between DCs of negative and positive offsets.

Then, we define the phase velocity deviation e_f at each frequency as:

$$e_f = \frac{abs |V - V_{avg}|}{V_{avg}} \quad (2.3)$$

Where V is phase velocity of the left or right dispersion curve at a certain frequency and V_{avg} shows the average phase velocity at the same frequency.

Furthermore, the averaged phase velocity deviation e_{avg} for each curve is:

$$e_{avg} = \frac{1}{N} \sum_{f=f_{min}}^{f_{max}} e_f \quad (2.4)$$

Where N displays the number of points having frequencies in range of $[f_{min} \text{ } f_{max}]$.

Numerical modeling and simulations can be helpful to partition the investigated media into different classes. However, here we will calculate the average value of e_{avg} along the seismic line, then we consider an upper-limit and a lower-limit as multiples of the averaged e_{avg} . Then, if e_{avg} of a dispersion curve is less than the lower-limit, the subsurface beneath the corresponding window is considered as low lateral variable. If e_{avg}

is more than the upper-limit, the corresponding portion of subsoil will be put in high lateral variable class. Finally, if e_{avg} of a dispersion curve is between lower and upper limits, the area beneath that window is considered as medium lateral variable.

2.4.2 Experimental uncertainty based on all shots

In order to obtain each single dispersion curve, several shots are used. Each shot generates a dispersion curve different from the other shots since the propagation path is different for each shot. As a result, for each frequency, we can have different values for phase velocity at each frequency. This is shown roughly in figure 2.8. These values, which are caused by experimental uncertainties, varies for each frequency within the frequency band. Here, our idea is to calculate the average value of experimental uncertainties for all dispersion curves retrieved from total offsets and display them as a function of window maxima location. This, in turn, can identify the portions of the seismic line in which the uncertainty is too high.

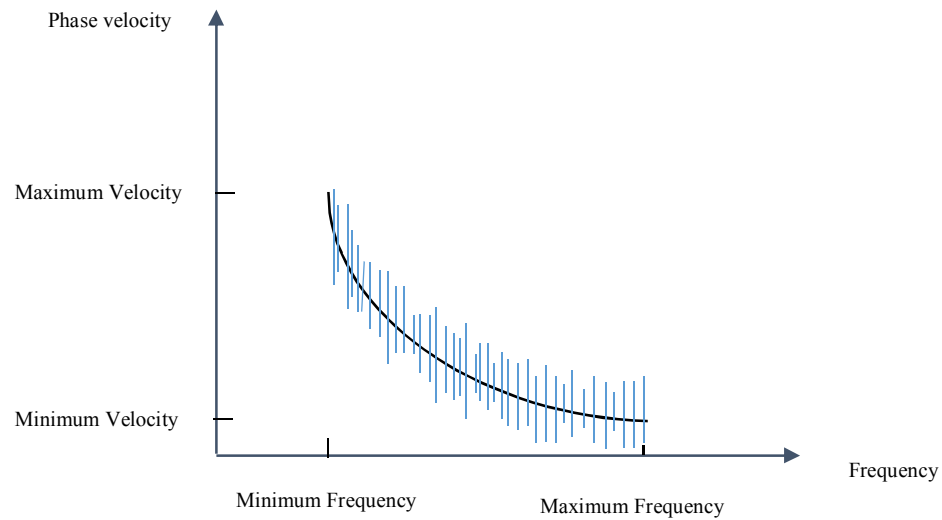


Figure 2.8. *Schematic example of experimental uncertainties in dispersion curves. Blue lines display uncertainties for each frequency. It can be seen that for each frequency, an interval of possible phase velocities exists. The black line represents the fundamental mode.*

In this work, we firstly calculate experimental uncertainties for all dispersion curves. Then, the average number for uncertainties will be calculated. Then, we define upper-limit and lower-limit as multiples of the obtained value for uncertainties. Afterwards, we consider areas with average uncertainties more than upper-limit as highly uncertain, the ones with uncertainty value less than the lower-limit, to be low uncertain and rest of them as medium uncertain.

2.4.3 Frequency bandwidth

Another index used for uncertainties evaluation is frequency bandwidth. We can assess frequency bandwidths of dispersion curves along seismic line. Then, we compute two thresholds based on the average value of frequency band. If the frequency bandwidth of a curve is less than the lower-threshold, we consider the DC to be highly uncertain. Moreover, if the frequency band is more than the upper-threshold, the corresponding DC is assumed to be reliable. Rest of the curves are classified as medium category.

Data, Processing and Results

3.1 Data

We do not reveal the location where the used data were acquired for confidentiality reasons but we provide a general description of the site. The data have been acquired onshore, along a 12 km line. The geological environment is a foothill zone and the line crosses some alluvial fans. The deposited alluvial debris on top of a sedimentary bedrock created a low velocity near-surface layer. A sketch of the seismic line and a previously estimated velocity model (Masoni, 2016) is shown in figure 3.1.

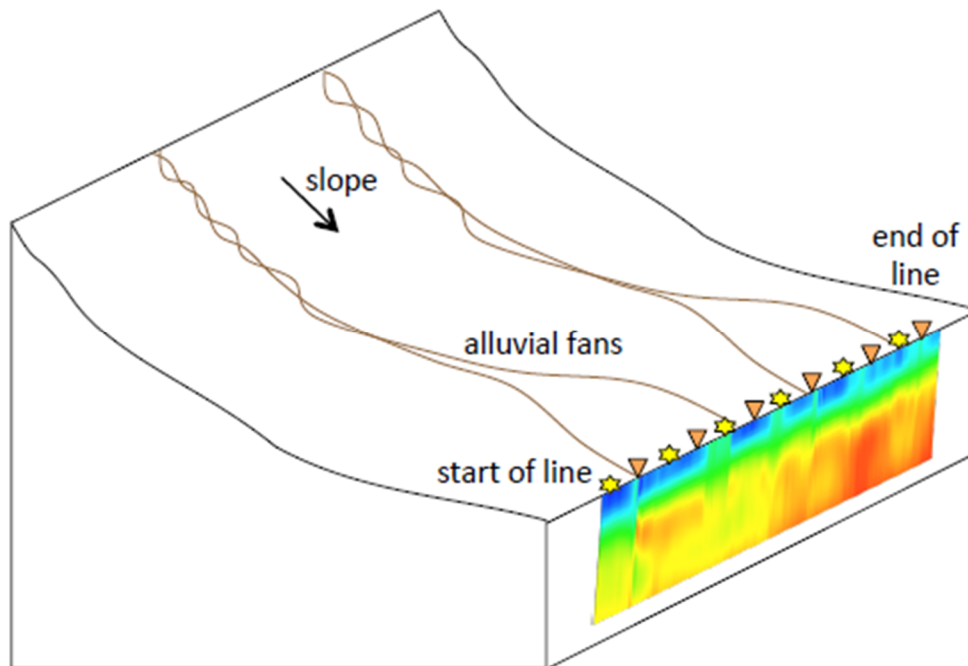


Figure 3.1. *Schematic picture of the location where the dataset was gathered (Masoni, 2016).*

It is known from previous studies that P-wave velocities, in the first 200 m of the subsurface, were in range of $2500\text{-}3500\text{ m/s}$. As a result, it was concluded from these high velocities that the investigated medium consists of compacted and hard formations.

The 12 km seismic line had an approximately flat profile with low topography variation. The dataset was acquired with 601 receiver groups with 20 m spacing and 600 shots with 20 m spacing. Each receiver group consisted of 12 vertical geophones with natural frequency of 10 Hz spaced 1.66 m apart. For each source, all receivers recorded four sweeps which were later stacked. The sweep has frequency band of 4 Hz to 90 Hz . Record length and sample interval in dataset acquisition were equal to 6 s and 2 ms , respectively.

3.2 Processing

The processing workflow described in the second chapter was applied to the seismic records. In the following we report some examples of intermediate processing steps outcomes and tests carried out to select optimum processing parameters

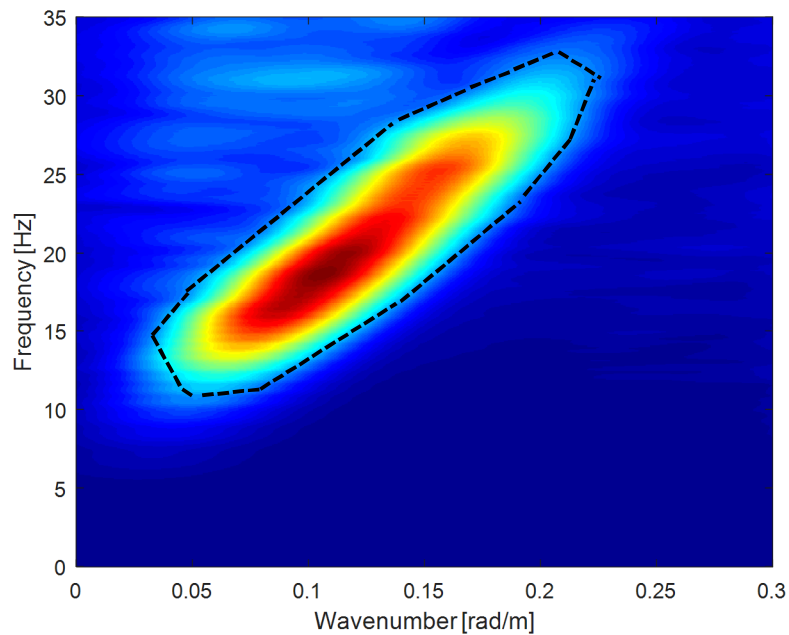


Figure 3.2. *The f - k spectrum of the window centered on 339th receiver.*

In figure 3.2, we pick the area with higher energy which can be recognized by its different colors from the background color, then we use this area, which is shown by dashed line, to retrieve the corresponding dispersion curve. In order to facilitate our work in picking process, we have used normalized f - k spectra. We show an example of normalized f - k spectra and the corresponding dispersion curve in figure 3.3

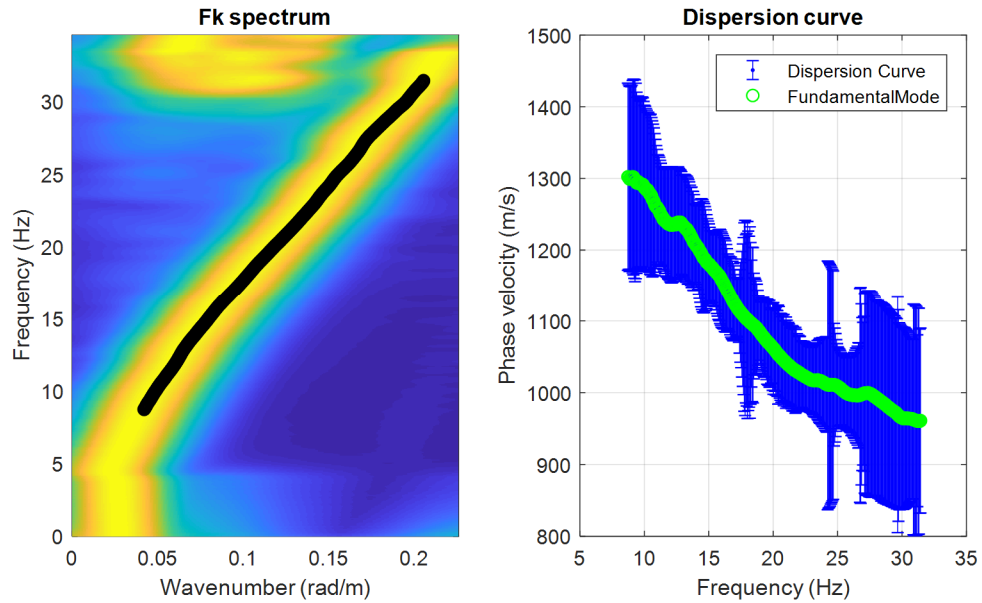


Figure 3.3. The f - k spectra alongside the DC of the Gaussian window with maximum locating on the 339th receiver. Here, the results relate to total offset.

The black line in the left part of figure 3.3 corresponds to dispersion curve at f - k spectra. The error-bar in the right graph originates from the experimental uncertainties. In other words, we have used 18 shots to generate the dispersion curve and each shot leads to different dispersion curve. So, we have a possible range for the dispersion curve which has been shown by blue area in the graph of figure 3.3. The experimental uncertainties have been estimated for all the retrieved dispersion curve, but in the following, we will omit the error-bar for eek of clarity when comparing dispersion curves.

3.3 Results

To satisfy the requirements of our processing approach, we have performed several tests. The goal is to get the optimized values for Gaussian windowing parameters such as: moving segment size L , overlap of adjacent segments ΔL , maximum offset range, minimum offset value and Gaussian window parameters α and β . After obtaining these values, we applied Gaussian windowing to our seismic data in order to retrieve dispersion curves. Finally, we have divided our subsoil into three categories based on QC parameters.

3.3.1 Determination of Maximum Allowable Source-Receiver Distance

We have carried out some tests on different intervals along the seismic line in order to get the furthest distance between the source and receiver which can produce high quality dispersion curves. The first test has been performed in the interval of 130th-180th receivers. A single shot at the left side of the interval has been considered in each step, starting with the closest shot followed by gradual increment of the distance. The first Gaussian window maxima located on 140th receiver and the dispersion curves corresponding to this window were analyzed in each step. We have observed that after a certain distance, the dispersion curves lose their continuity at high frequencies. Besides, as we went further from the receivers, this discontinuity occurred in lower frequencies. In other words, the frequency band decreased as the offset increased.

In figure 3.4, some dispersion curves from this interval have been depicted.

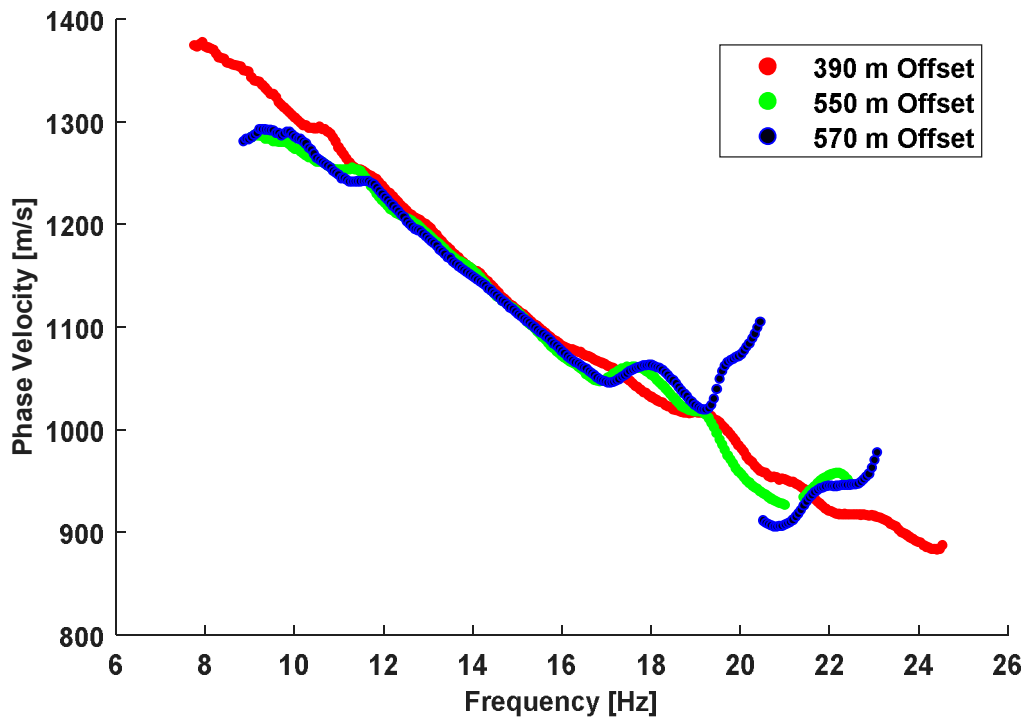


Figure 3.4. Dispersion curves of the Gaussian window centered on the 140th receiver for shots at: 390 m, 550 m and 570 m.

As shown in figure 3.4, the dispersion curves for the shots at 390 m and 550 m have almost the same trends and frequency bands while for the shot at 570 m, the frequency above 18 Hz are unstable. As a matter of fact, the dispersion curves corresponding to the shots less than 570 m far from the 140th receiver showed acceptable continuities and frequency bands. Therefore, the selected value for the maximum allowable distance between shot and receiver in this interval was 550 m.

The above test has also been carried out in the interval of 270th-320th receivers. In figure 3.5, the dispersion curves of the window with maxima locating on 280th receiver have been displayed.

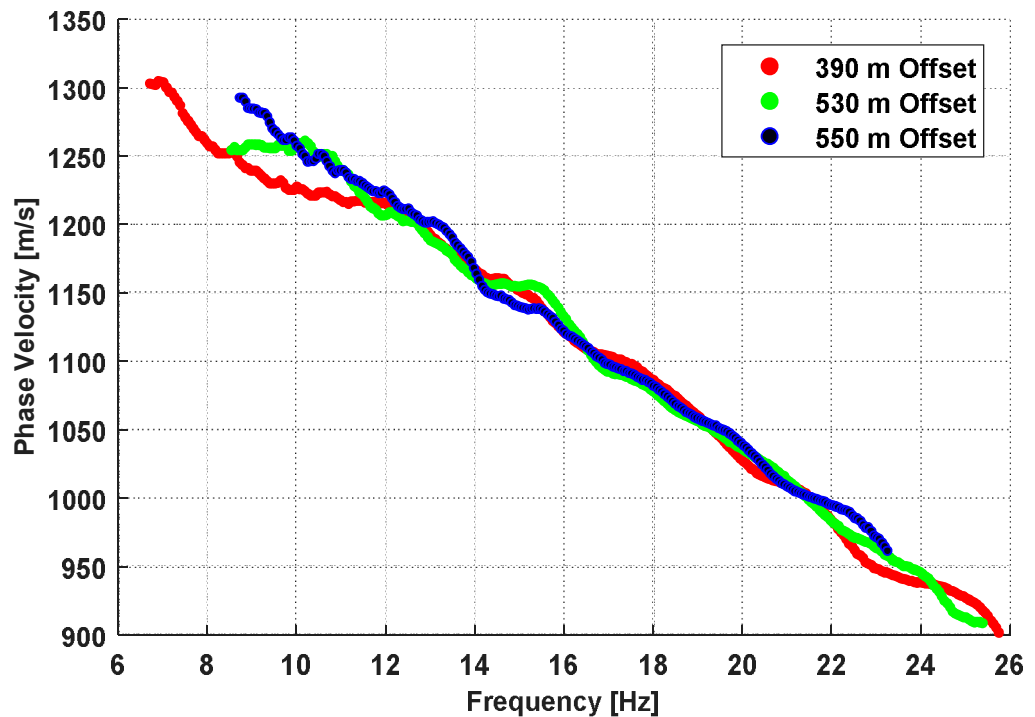


Figure 3.5. Dispersion curves for the Gaussian window centered on the 280th receiver for shots at: a) 450 m b) 530 m and c) 550 m.

We can clearly see that the dispersion curves of offsets at 390 m and 530 m have had approximately the same frequency bands, but in case of 550 m offset frequency band is narrower. So, 530 m was considered as the optimum value for the furthest acceptable offset at this interval.

Two other similar experiments in different intervals were carried out. The results for different intervals were almost at the same range. To take maximum caution, we have selected the lowest number among the obtained values, as the maximum acceptable distance between source and receiver. As a result, the selected value for the maximum distance between the shot and receiver was set to 510 m (figure 3.6).

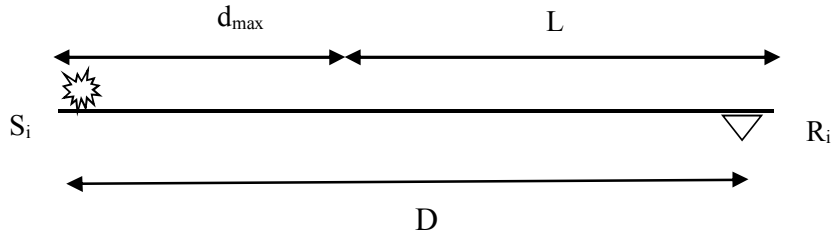


Figure 3.6. Scheme of maximum offset test. D is the maximum acceptable distance between the shot S_i and receiver R_i . 510 m is the selected number for D which should be divided between receivers segment size L and maximum offset d_{max} .

3.3.2 Determination of Minimum Acceptable Offset

The procedure to find the minimum offset range to be used in stacking process, was similar to what we have discussed earlier in case of maximum offset determination. Because of near-field effects, we have examined dispersion curves retrieved from shots at near offsets. Figure 3.7 has shown the corresponding results in the interval of 130th-180th receivers.

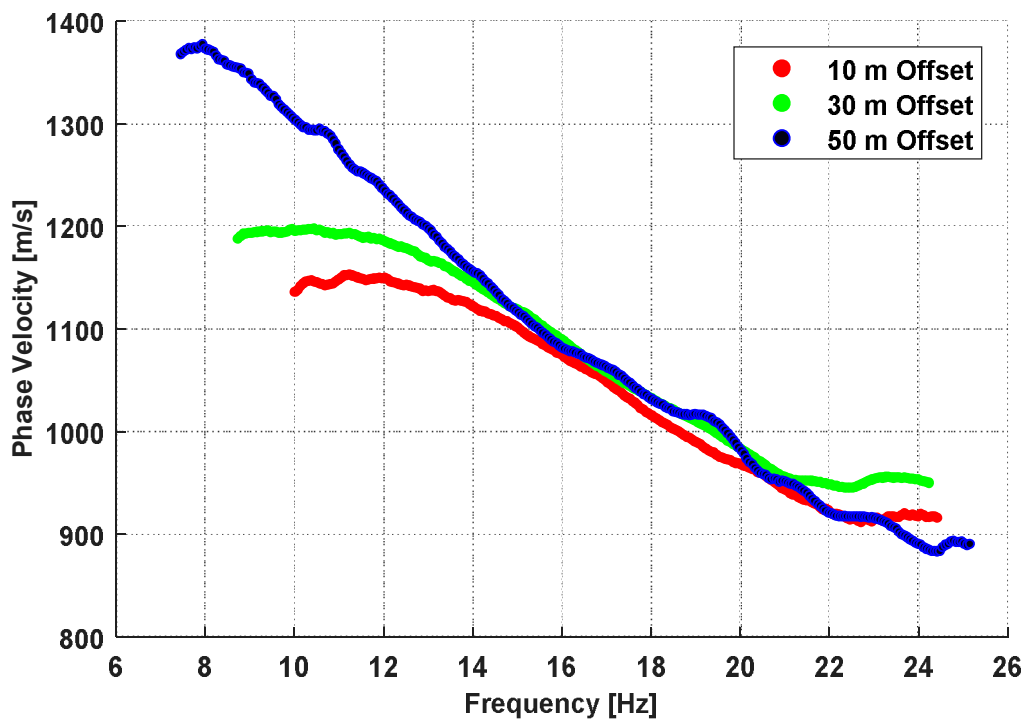


Figure 3.7. Minimum offset determination based on the dispersion curves of shots at: a) 10 m, b) 30 m and c) 50 m.

In figure 3.7, the dispersion curves at 10 m and 30 m offsets have narrower frequency bands than DC at 50 m offset. Moreover, the trends of dispersion curves at 10 m and 30 m offsets were different from the other shots particularly in low frequencies. However, the third curve was more consistent with results of other shots.

Results of similar tests in intervals of 270th-320th and 420th-470th receivers also have confirmed the above conclusion. As a result, the minimum offset to be used in further designs was selected equal to 50 m.

3.3.3 Segment Size L

Based on our previous results, we have selected 510 m as the maximum distance between shots and receivers. Having known that the spacing between two adjacent shots (or receivers) was 20 m, the number of receivers in segment cannot be more than 25 receivers. Besides this, we needed to give a certain portion of the aforementioned 510 m to the shots.

So, several tests have been designed to pick the best value for number of receivers. We have analyzed different window sizes with 15, 10 and 20 receivers. At the end, we came up to choose 15 receivers for future designs. This, in turn, led to get the maximum offset equal to 210 m.

3.3.4 Determination of Alpha and Beta

One important factor in Gaussian windowing design is the value of α . Since the length of our seismic line was 12 km which was really a long line, we performed several tests in different portions of the survey line. An example of these tests is shown in figure 3.8. As it can be seen in the figure, the minimum needed wavenumber resolution is a bit more than 0.04 rad/m.

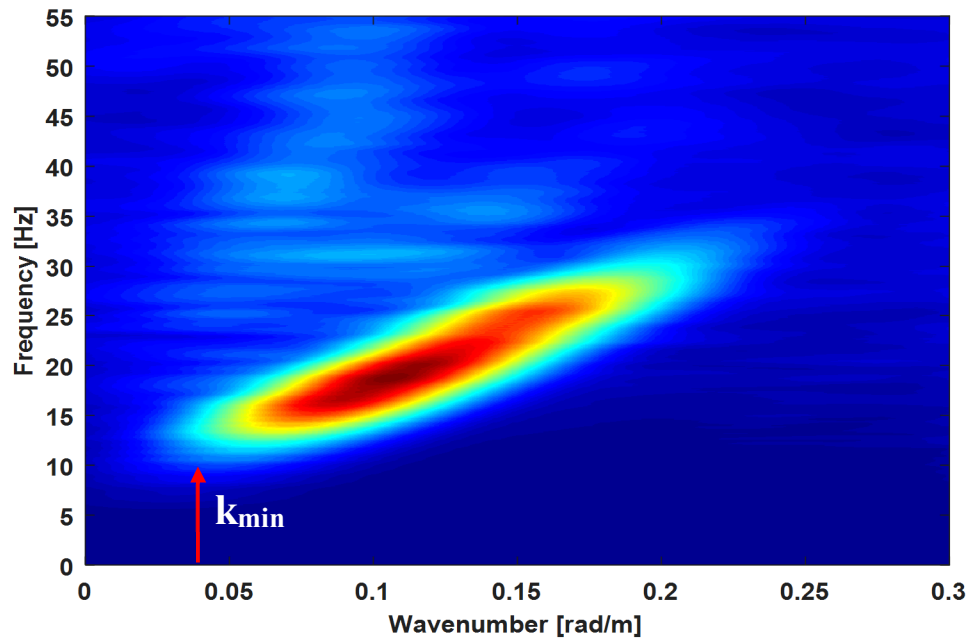


Figure 3.8. *Example of wavenumber resolution determination.*

Having known the wavenumber resolution and number of receivers in each line segment, the corresponding value for α can be determined by using figure 3.9.

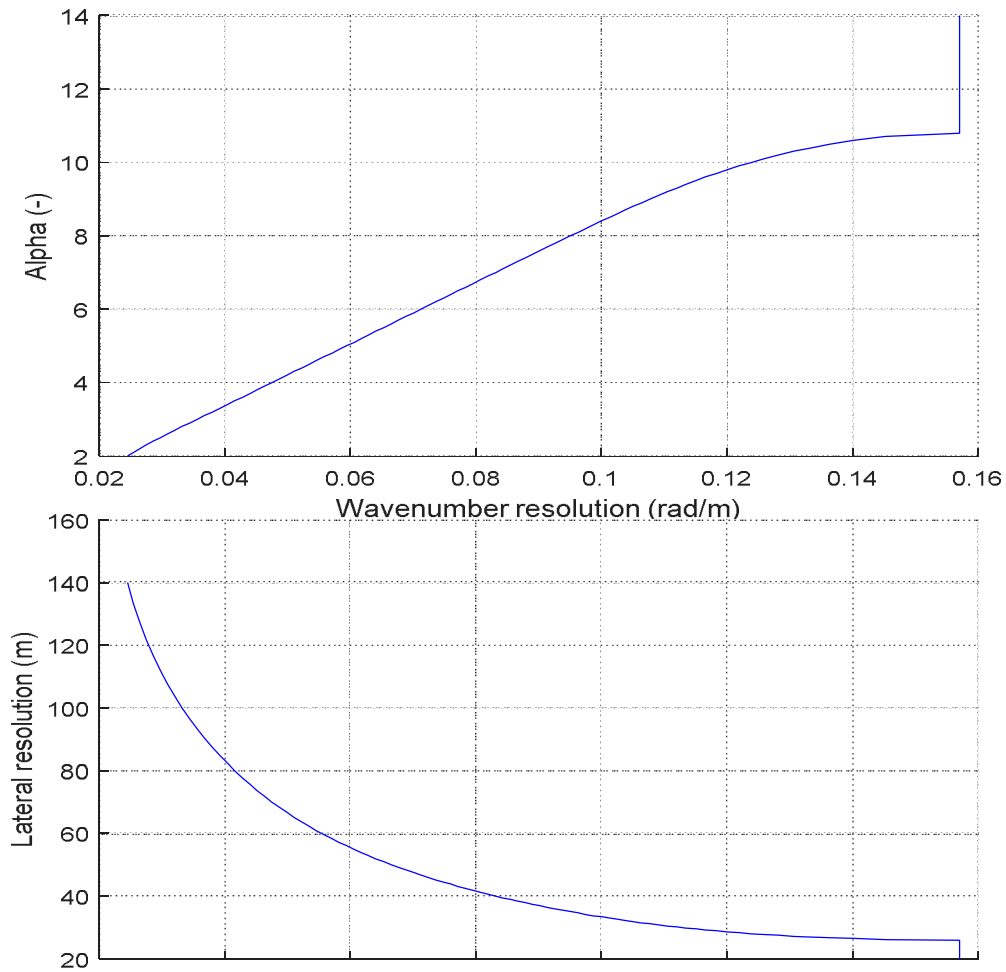


Figure 3.9. *Lateral resolution and f - k spectra resolution in case of 15 receivers.*

Based on figure 3.9, to satisfy the needed wavenumber resolution, α should be almost 4.

Having known the value of α and wavenumber resolution, we were able to determine the lateral resolution through the lower plot of figure 3.9. So, the guaranteed lateral resolution is equal to 75 m but we selected a lower number of lateral resolution leading us to a denser dispersion curves extraction. We have considered a curve every 60

m to investigate the lateral variation more carefully. It has been mentioned earlier that β is a number in range of 0 to 1, and it represents the location of window maxima in receivers segment. According to our design, there are 15 receivers in each line segment. Based on the chosen value for α , the first window maxima locates on the 5th receiver of each segment. Since we have selected a window each 60 m, there are two other windows in each segment with window maximum located on 8th and 11th receivers. As a result, the values of β in each segment are equal to 0.33, 0.53 and 0.73.

3.3.5 Overlap of Adjacent Segments

Spatial windows needed to overlap to enable us to retrieve the dispersion curves representative of the whole seismic line. So far in our design, we have selected intervals with 15 receivers and α equal to 4. It meant that we might lose information at the edge of each single interval. For example, in the first interval we had three windows and the last window maxima located on the 11th receiver and the first window of the next interval had its maxima on the 19th receiver. So, we observed a gap between every two adjacent intervals.

To avoid this problem, we have considered *120 m* overlap of the spatial windows which was equivalent to 6 receivers. As a result, the second interval started from 9th receiver to the 23rd and the maxima of its first window located on the 14th receiver. As a result, we have removed the gap between the two adjacent intervals by applying *120 m* of overlap between these two adjacent intervals.

3.3.6 Final Design for Dispersion Curve Extraction

So far, different needed parameters for extraction of dispersion curves have been acquired. We have outlined the information about our design along the survey line in table 4.1.

Seismic Line Length (km)	Considered Line Segments	Sources per Line Segment	Sources per Line Segment
12	66	15	18
Windows per Line Segment	Extracted DCs per window	Total windows	Total retrieved DCs
3	3	198	594

Table 4.1. *Summary of seismic line division into intervals.*

3.3.7 Retrieved Dispersion Curves

We have processed the data according to our final design and then we extracted dispersion curves along the survey line. Figure 3.10 displays the pseudo-section of total offsets along the seismic line.

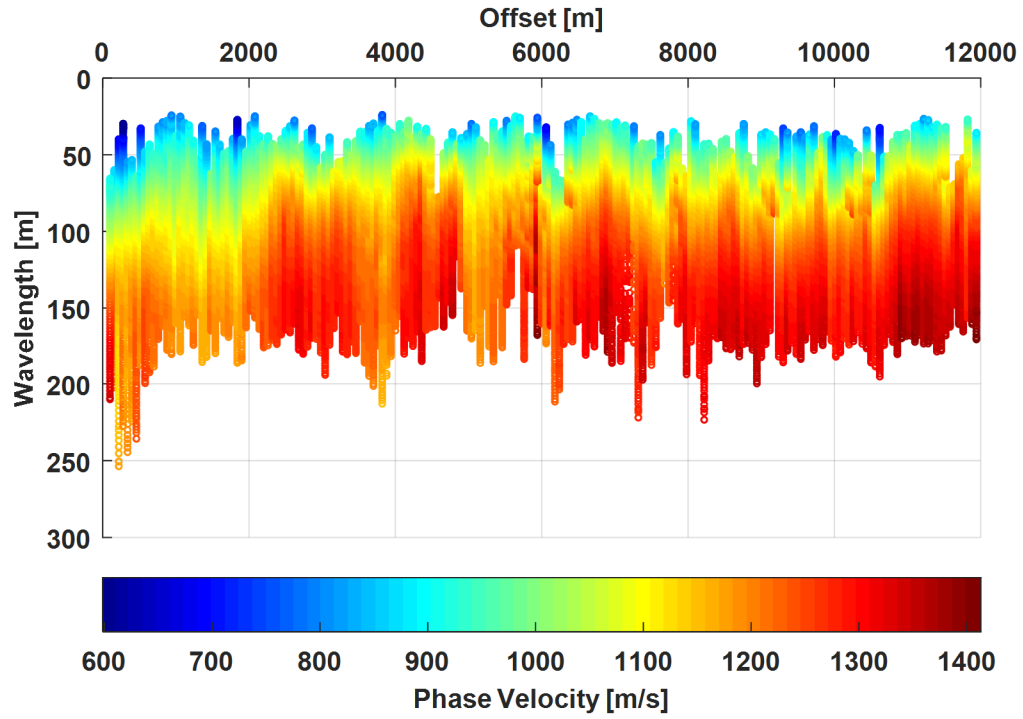


Figure 3.10. *Pseudo-section corresponding to total offsets.*

The dispersion curves retrieved from the total offsets have been plotted together in figure 3.11.

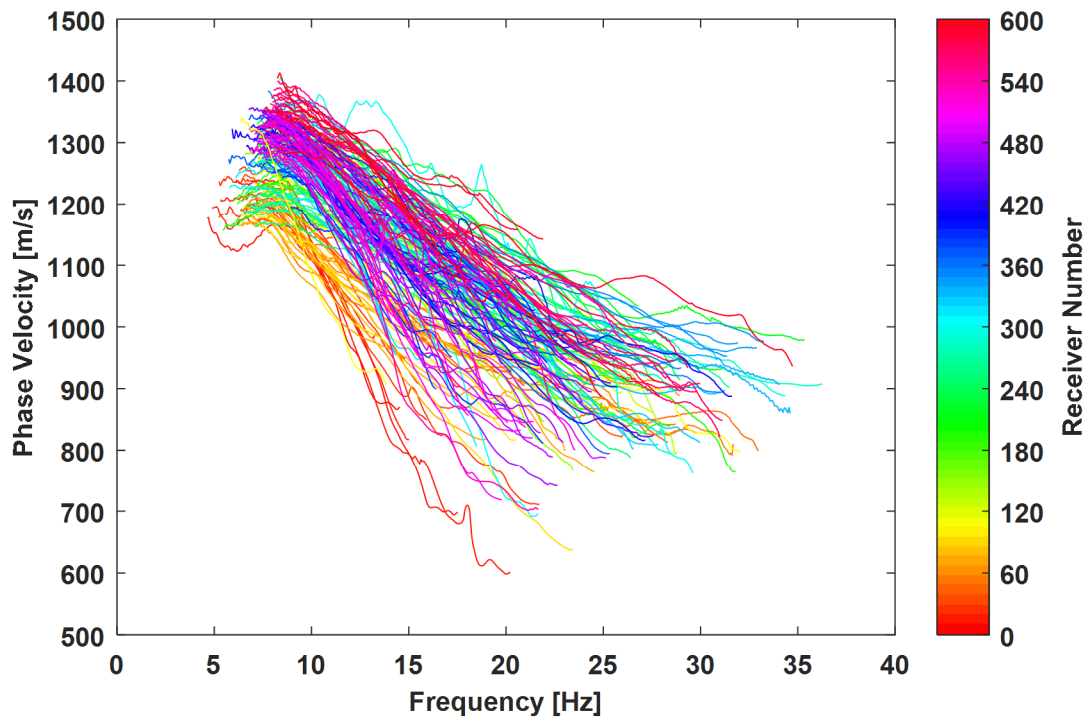


Figure 3.11 .All the retrieved dispersion curves related to total shots along seismic line.

All the retrieved dispersion curves from the positive offsets have been shown together in figure 3.12.

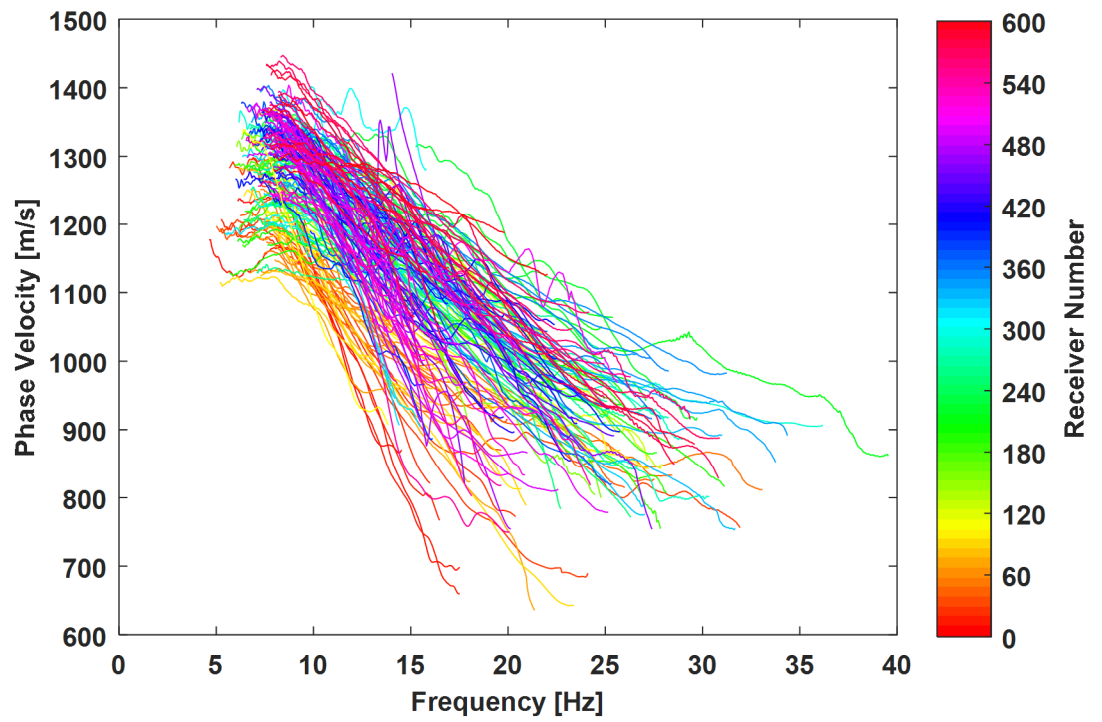


Figure 3.12. *All of the obtained dispersion curves from positive offsets along seismic line.*

All of the dispersion curves obtained from negative offsets have been presented altogether in figure 3.13.

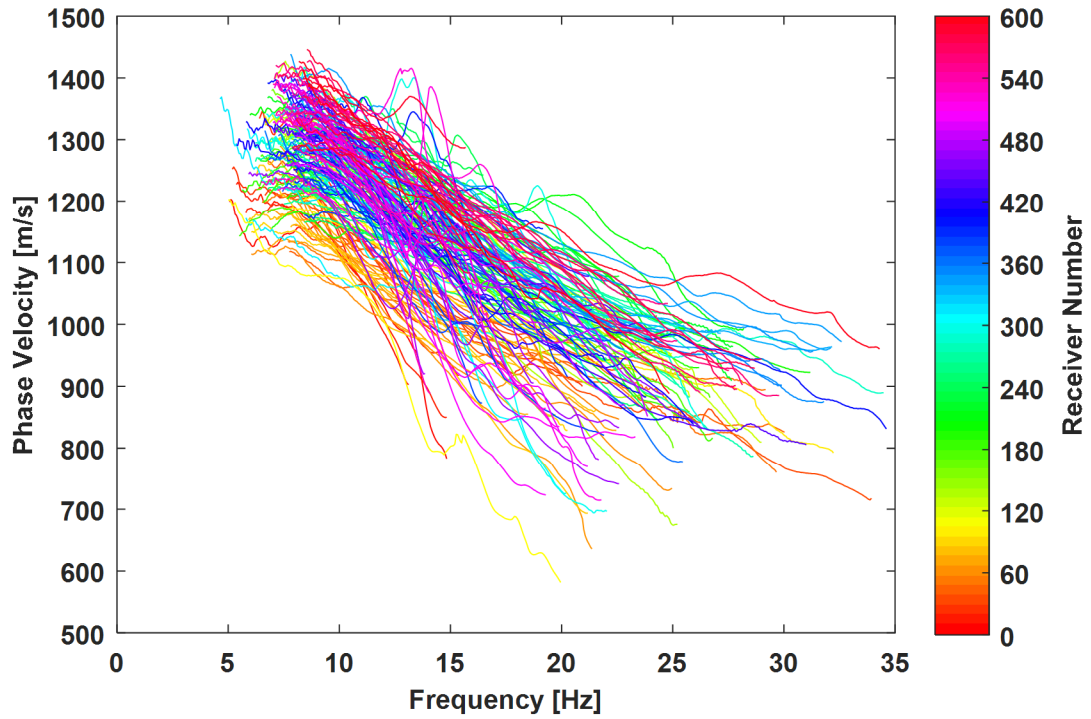


Figure 3.13. *All the dispersion curves obtained from left shots along seismic line.*

3.4 Quality Control Results

In this section, we check the quality of the extracted dispersion curves by using several indices. They can be used to select high quality curves later for inversion.

3.4.1 Experimental Uncertainty based on Sources on each side

We have applied the identified processing parameters to the whole seismic line.

In figures 3.14_3.17, several examples of the misfit between retrieved dispersion curves of negative and positive offsets have been depicted.

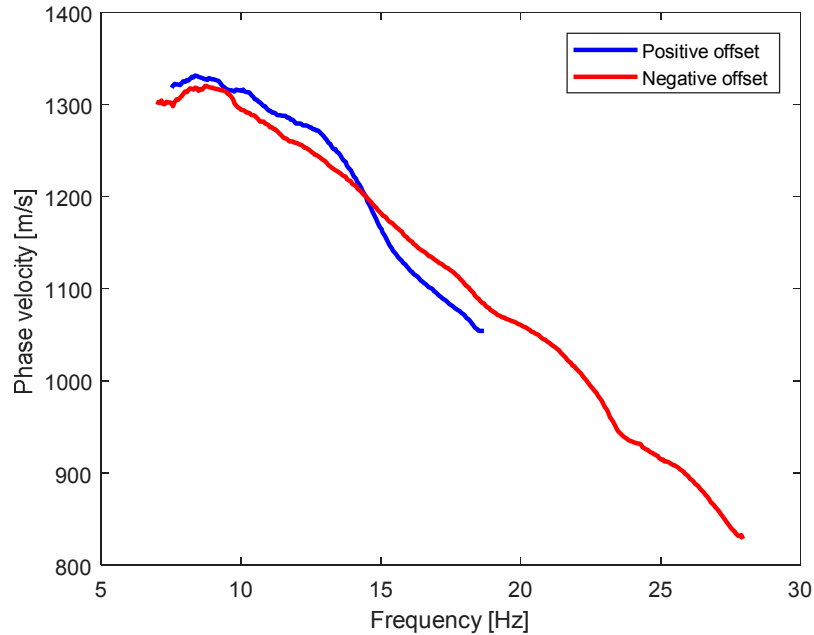


Figure 3.14. *Dispersion Curve of the Gaussian window with maxima located on 134th receiver.*

In figure 3.14, we observe that positive and negative offsets led to approximately equal dispersion curves in the frequency band 7 - 19 Hz. The dispersion curve corresponding to negative offset stopped at 19 Hz, however the positive offset one has covered frequencies as high as 27 Hz. This difference in frequency bandwidth in vicinity of the 134th receiver can be because of lateral heterogeneity at that area.

Another interesting result is plotted in figure 3.15:

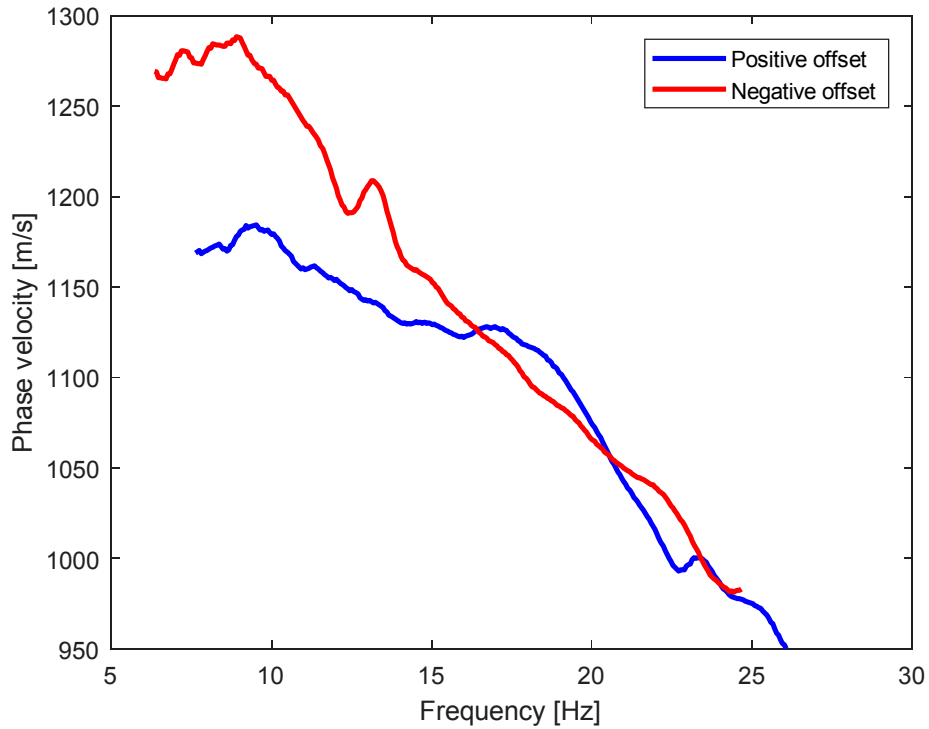


Figure 3.15. *Dispersion curve of the Gaussian window centered on the 200th receiver.*

In figure 3.15, misfit between positive and negative offset DCs occurs at low frequencies. The DCs fit in frequency band 16 -25 Hz while in 7-16 Hz the phase velocities differ significantly. Since low frequencies represent deeper parts of subsurface, we have concluded that uncertainties exist in vicinity of the 200th receiver particularly in higher depths.

We see also another type of misfit between the DCs in the window centered on 525th receiver in interval of 515th-529th receivers (figure 3.16).

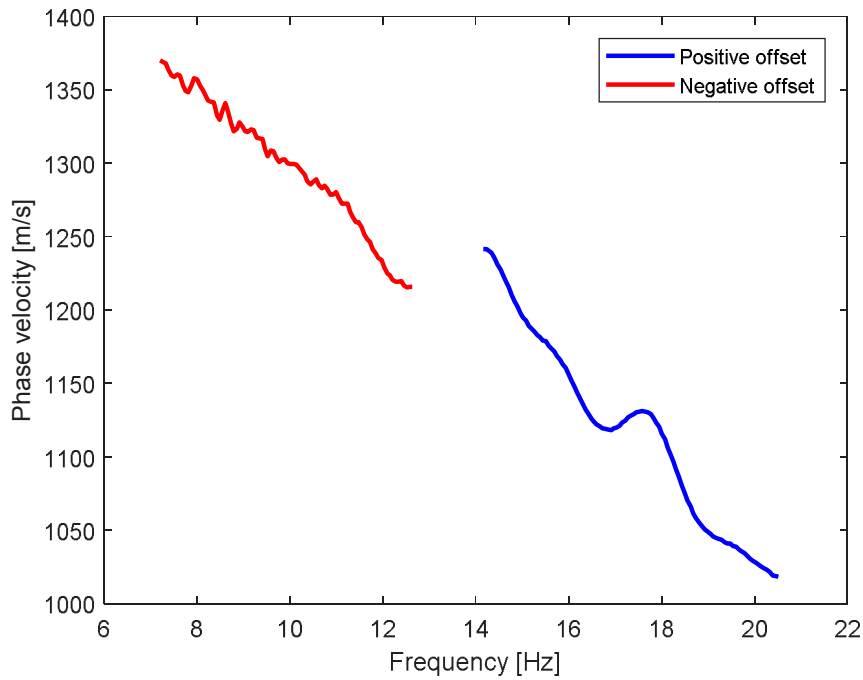


Figure 3.16. *The retrieved DC of the Gaussian window centered on the 525th receiver.*

In figure 3.16, the frequency range for positive offset was from 7 Hz to 13 Hz while the negative offset has covered frequencies of 14-21 Hz. So, we expected high degree of uncertainties in this location since the negative and positive offsets have produced completely different DCs.

In the following, for each window, the phase velocity deviation e_f from the average phase velocity at each frequency was calculated for the dispersion curves corresponding to positive and negative offsets. The next step was to get the average value for phase velocity deviation e_{avg} for each window.

Two examples of low and high values for e_{avg} , have been plotted in figures 3.17 and 3.18, respectively.

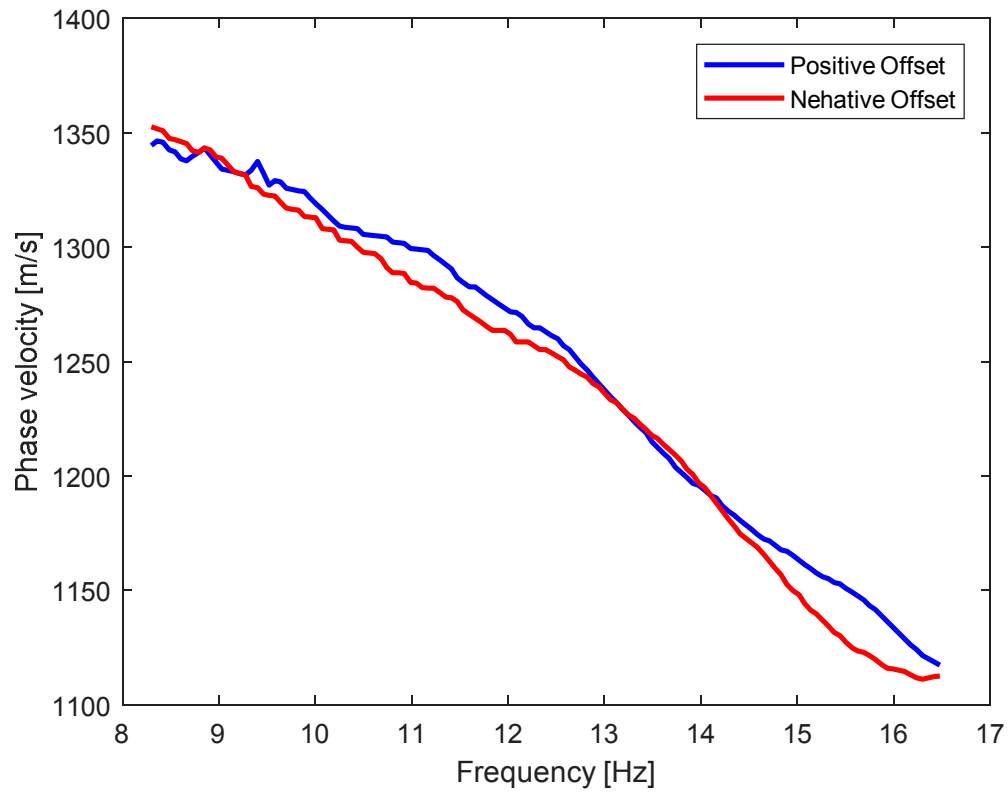


Figure 3.17. An example for low phase velocity deviation which occurs at 423rd receiver.

This location has showed the minimum number of e^{avg} along seismic line.

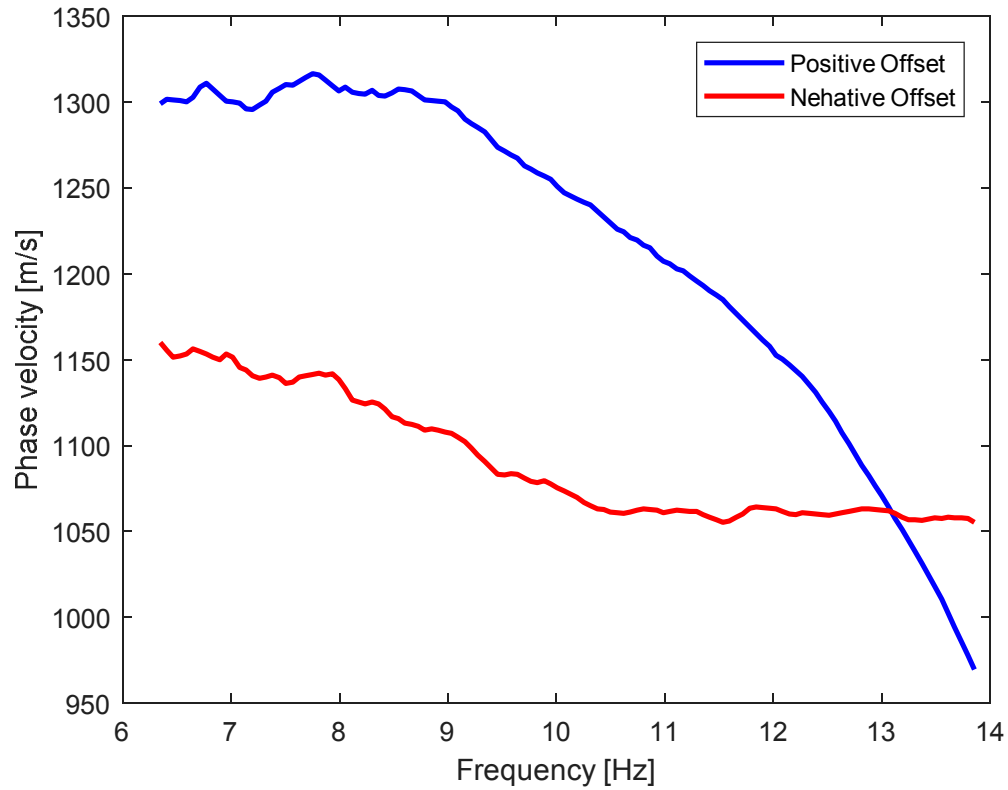


Figure 3.18. *The dispersion curves of Gaussian window centered on 312th receiver. Here, the observed value of the phase velocity deviation is among the highest numbers in the investigated media.*

The variations of e_{avg} along the survey line has been shown in figure 3.19.

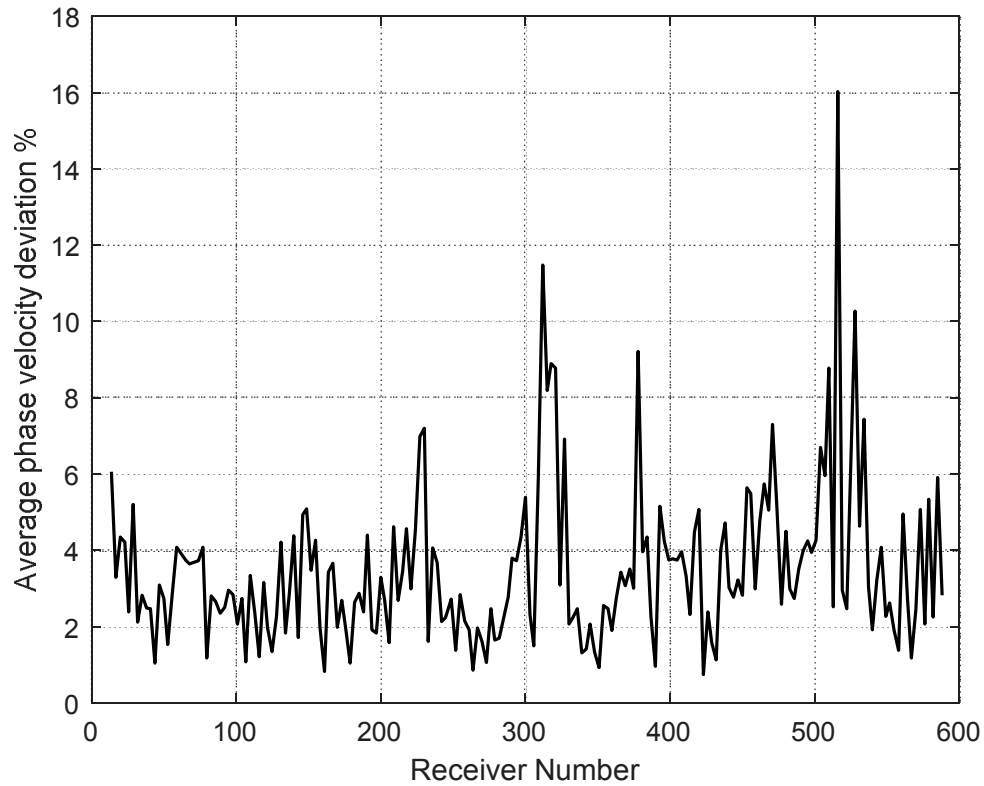


Figure 3.19. Average phase velocity deviation along the seismic line.

The average value for e_{avg} was 3.47 % where the minimum and maximum numbers were 0.73% and 16.03%, respectively. We divided our subsurface into three categories based on the results of figure 3.19. If the value for the average phase velocity deviation e_{avg} was less than $0.8 * e_{avg}$, that area has been considered to have low uncertainty level, and if this number was more than $1.2 * e_{avg}$, the corresponding location was selected as highly uncertain. Those windows having e_{avg} in the range of $0.8 * e_{avg} - 1.2 * e_{avg}$, were classified in medium uncertainty class.

The following pie chart displays the distribution of our subsurface into the three aforementioned categories:

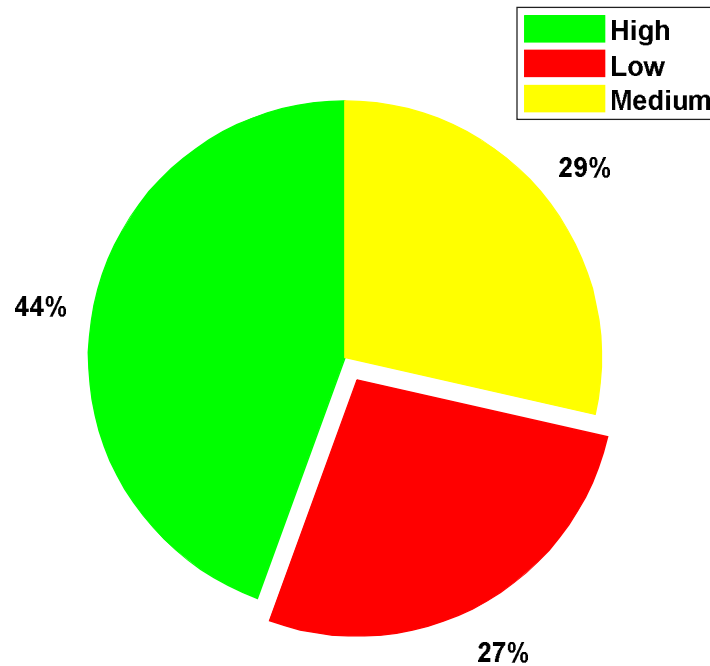


Figure 3.20. *Division of survey line into low, medium and high quality categories. There are 86 curves in high quality class, 54 curves in medium and 52 curves in the low quality category.*

In order to see the average phase velocity deviation e_{avg} as a function of location of dispersion curve, we have plotted figure 3.21 in which low, medium and high quality curves have been displayed by red, yellow and green dots, respectively.

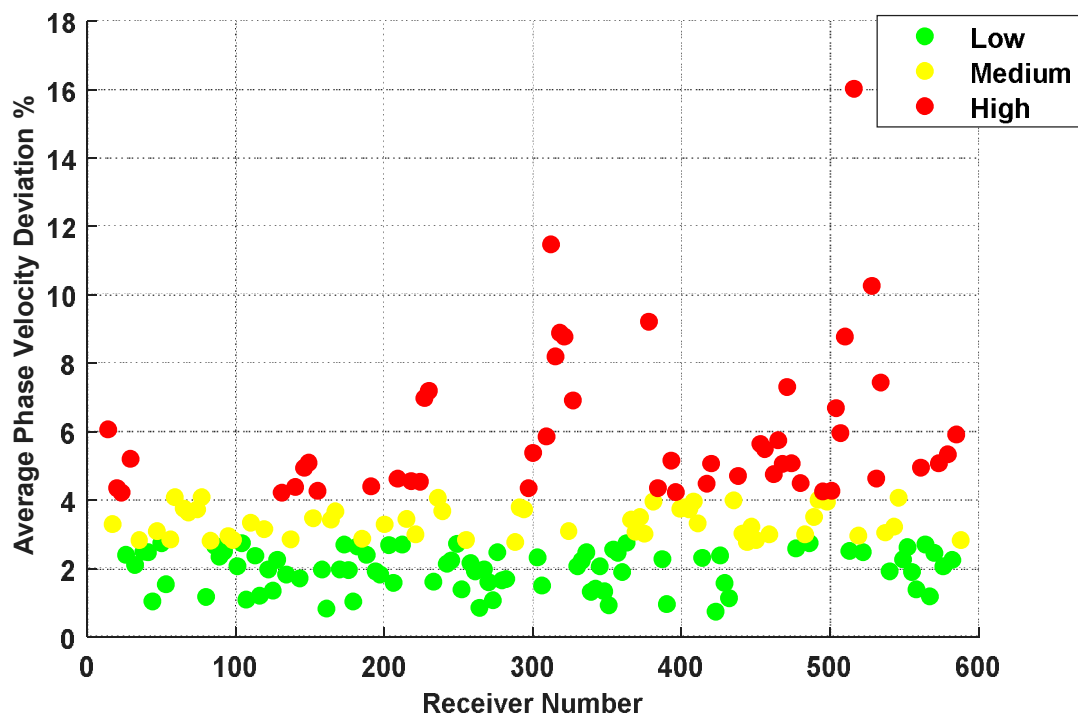


Figure 3.21. *Distribution of the average phase velocity deviation along the seismic line.*

Figure 3.21 enables us to have a quick overview of the DCs quality. For instance, we clearly observe high concentration of red points in vicinity of 300^{th} receiver. Therefore, it is expected to have low reliable curves in that area. Moreover, only a few green points can be seen close to receivers existing in range of $430-530$ and we mainly have yellow and red points in this interval. So, this area is also another candidate for low degree of curves reliability. Another interesting result occurs in the interval of $50^{th}-215^{th}$ receivers in which there are only a few red points and lots of green ones. As a result, we probably have high quality of dispersion curves in this portion of the survey line.

3.4.2 Experimental Uncertainty based on all Shots

We have used many shots to retrieve each dispersion curve. So, considering any window along the seismic line, there is a range of phase velocity for each frequency. An example of these ranges of phase velocities have been shown before as error-bars in figure 3.3. In this part, we have investigated the variation of this kind of uncertainty along the seismic line by averaging the uncertainties for each window and plotting the results along survey line (figure 3.22). The average value for experimental uncertainties is 13.63%. Here, we have defined upper-limit equal to $1.2 * Avg_{uncertainty}$ and lower limit equal to $0.8 * Avg_{uncertainty}$. Here, a curve considered as highly uncertain if its uncertainty exceeds the upper-limit. If the uncertainty is less than the lower-limit, the curve is assumed to be reliable. Otherwise, it is categorized as medium uncertain.

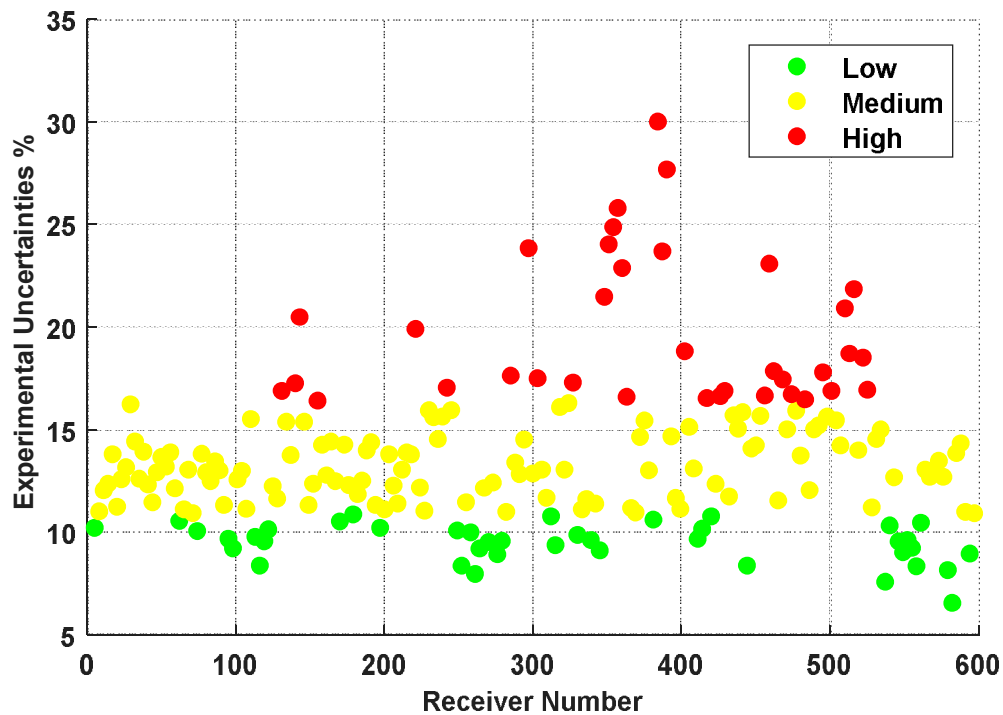


Figure 3.22. *Experimental Uncertainties as a function of window maxima location.*

3.4.3 Experimental Uncertainty based Frequency Bandwidth

Minimum and maximum frequencies as well as frequency bandwidths of total offsets DCs are shown in figure 3.22.

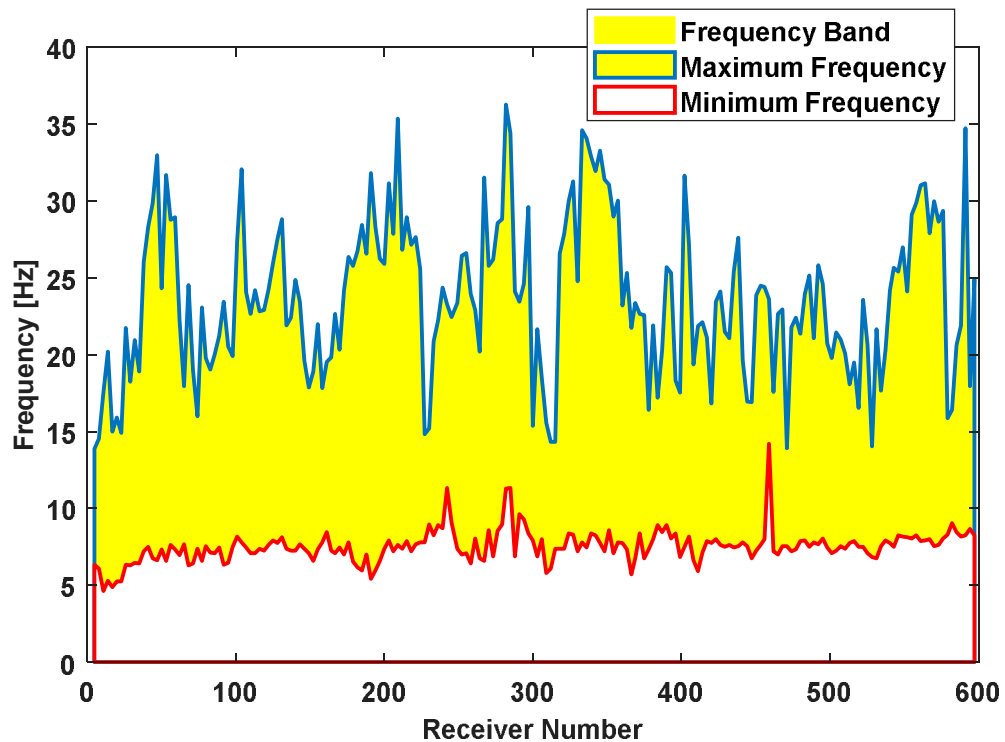


Figure 3.22. *Minimum frequency, maximum frequency and frequency band of total offsets along the seismic line.*

The computed value for average frequency band is 16.10 Hz. Likewise the previous section, we divide the curves into three classes: highly reliable, medium and low reliable.

Again, we use two limits based on the average frequency band to categorize the DCs. Lower-limit is $0.8 \cdot \text{Avg}_{\text{fband}}$ and upper-limit is equal to $1.2 \cdot \text{Avg}_{\text{fband}}$. Figure 3.23 shows the three groups of curves based on their frequency bandwidths.

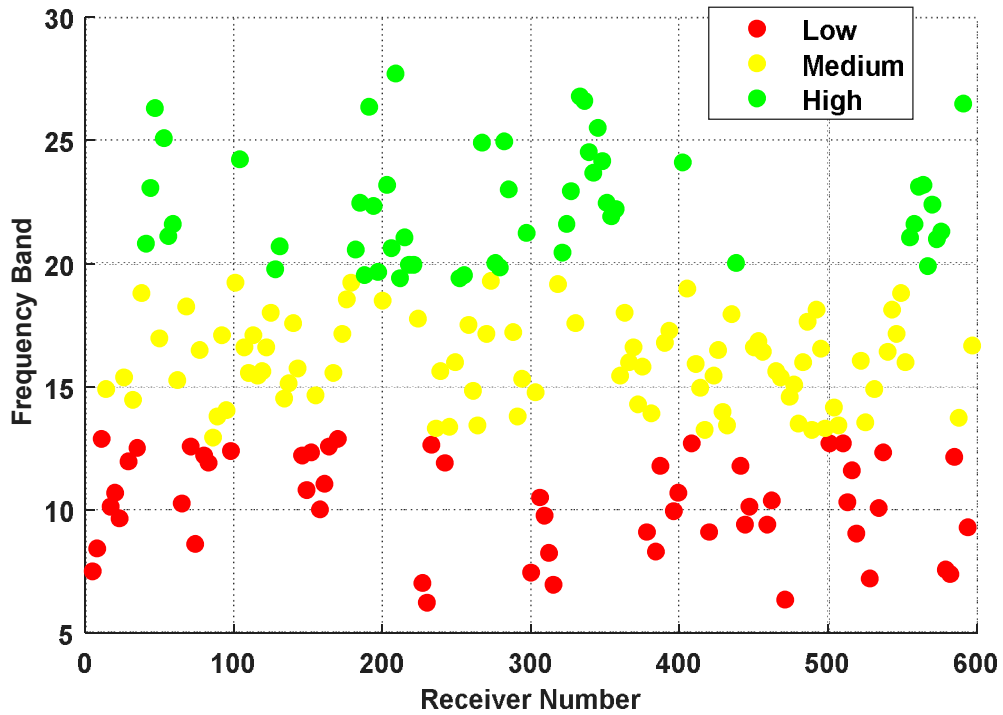


Figure 3.23. Frequency band as a function of receiver number. Red dots represent highly unreliable curves and green color is used for reliable DCs and yellow displays medium class.

3.4.4 Cross-plots of Uncertainty Indices

So far, we have introduced three indices for QC and applied them separately to investigate the degree of uncertainty along the survey line. In this section, we combine the results of those indices in figures 3.24_3.26. If a curve is considered highly unreliable in

both methods, it will be shown by red, and if it in reliable class of both indices, it will be displayed by green color in the figures. Otherwise, the curve is considered as medium class which will be represented by yellow.

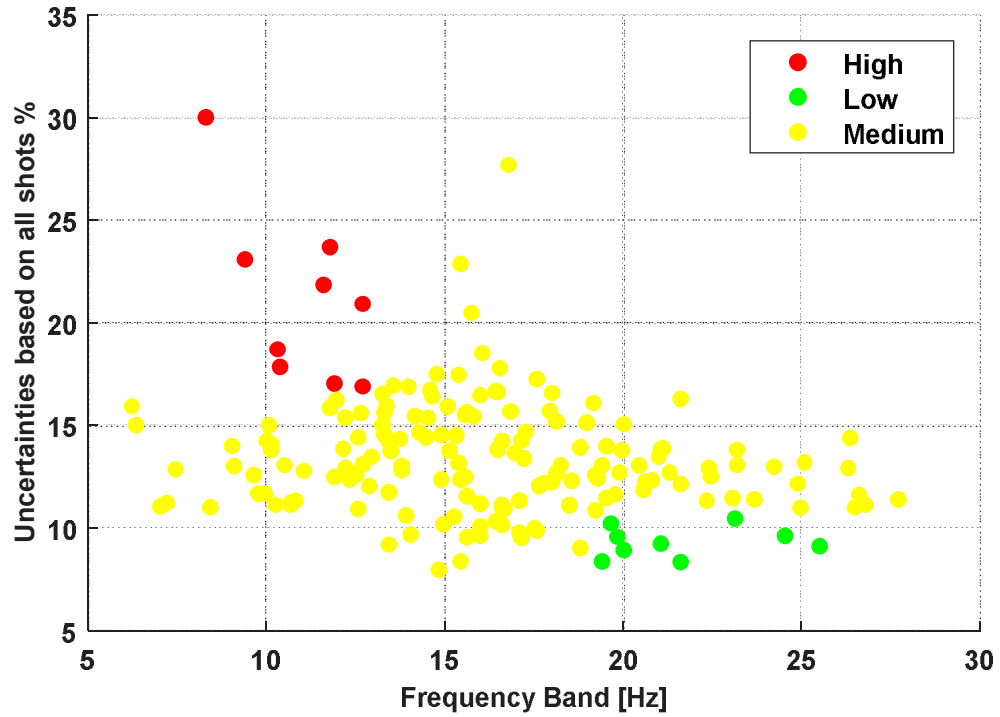


Figure 3.24. *Cross-plot of experimental uncertainties based on all shots and frequency bandwidths.*

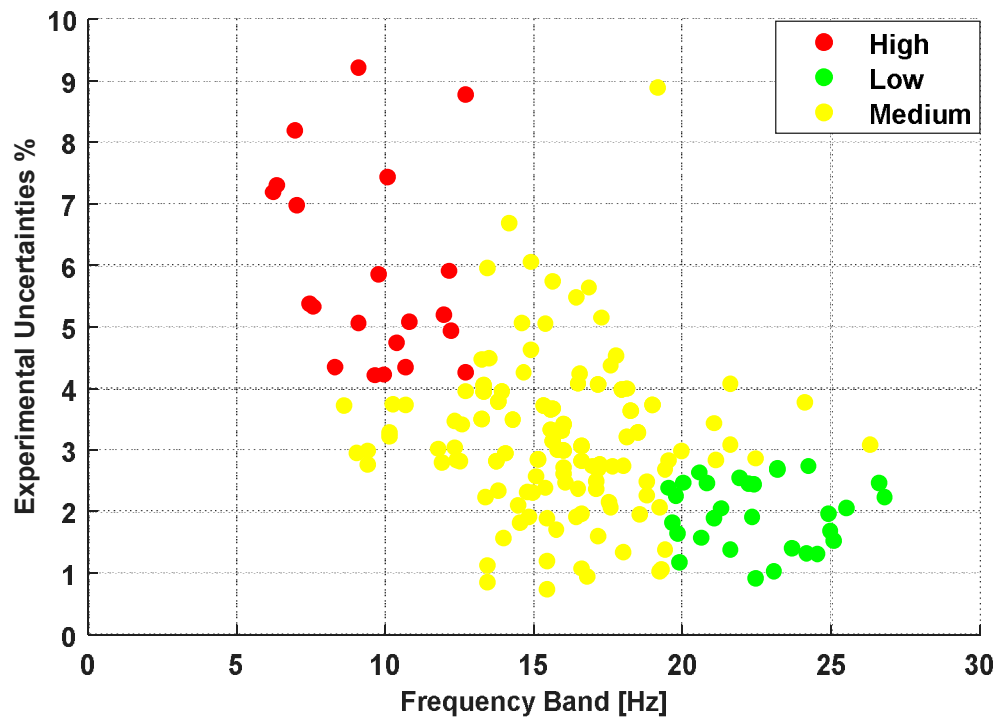


Figure 3.25. *Cross-plot of phase velocity deviations and frequency bands.*

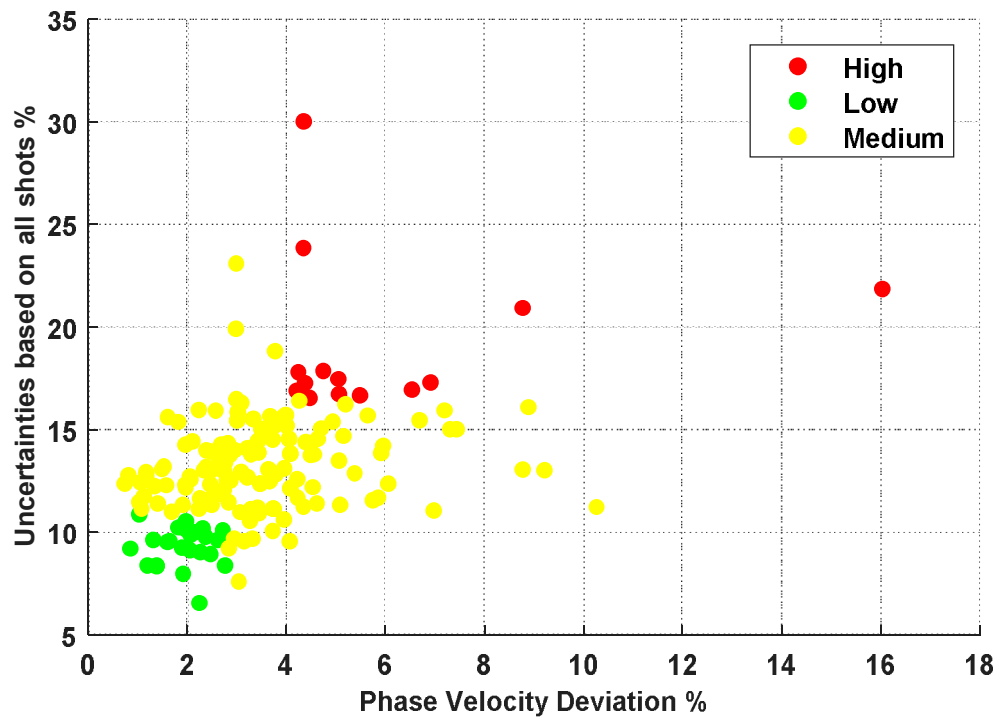


Figure 3.25. *Cross-plot of uncertainties of shots on each side and phase velocity deviations.*

Figure 3.26 displays all three uncertainty indices in a single 3D plot.

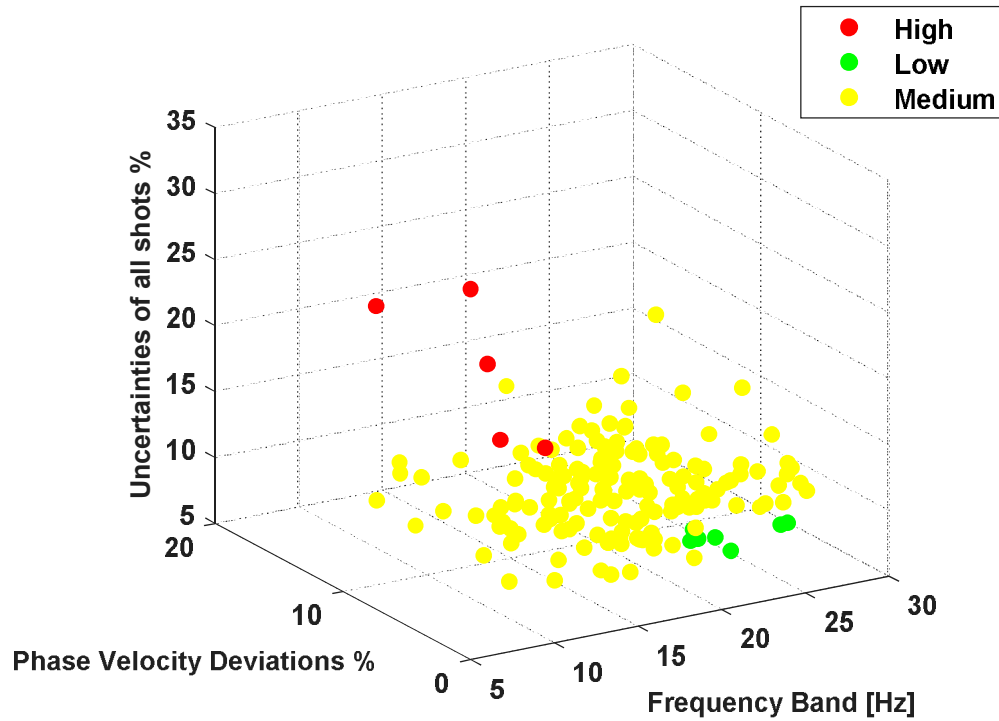


Figure 3.26. *Cross-plot of the three uncertainty indices.*

As we can see in figure 3.26, there are only a few curves which are highly unreliable in all three methods. Likewise, high quality curves in all methods are not numerous and we mainly have curves with medium reliability.

Conclusions

Surface Wave method is a powerful tool to retrieve velocity models. We have defined a processing workflow based on seismic line segmentation and windowing with a moving Gaussian window. Dispersion curves are extracted in f-k domain and stacking of f-k spectra is used to increase the signal to noise ratio. The workflow has been applied to a *12 km* seismic line acquired for oil and gas exploration purposes in a foothill environment where high heterogeneities of the weathering layer is expected. First we have optimized the processing parameters that define segmentation, windowing and source offset on the basis of a series of tests carried out on the data. Then we have extracted all the dispersion curves.

The obtained dispersion curves have an average bandwidth of *16.10 Hz* and a phase velocity range from *598 m/s* to *1413 m/s*. This leads to a wavelength range of *24 m- 253 m* that roughly means an investigation depth around *172 m*.

Due to the high heterogeneity of the near surface layers, the obtained dispersion curves have heterogeneous quality along the line. To identify critical zones and provide a tool to select those dispersion curves that can be inverted and those that might be discarded due to poor quality or inconsistencies, we have defined 3 QC parameters: i) the misfit between dispersion curves obtained by using positive and negative offset, ii) the experimental uncertainties computed over a population of shots for each window position, iii) the bandwidth. These QC parameters have been plotted along the line and cross-plotted among each other. The analysis of the QCs have shown that they identify properly critical zones.

The workflow and the QC open to the processing of surface wave present in seismic exploration dataset in an efficient way that could be implemented in industry workflows.

References

- Bergamo, P., D. Boiero, and L. V. Socco, 2012, retrieving 2D structures from surface-wave data by means of space-varying spatial windowing: *Geophysics*, 77, no. 4, EN39–EN51, doi/; 10.1190/GEO2012-0031.1.
- Bohlen, T., S. Kugler, G. Klein, and F. Theilen, 2004, 1.5D inversion of lateral variation of Scholte wave dispersion: *Geophysics*, 69, 330–344, doi: 10.1190/1.1707052.
- Boiero, D., and L. V. Socco, 2011, the meaning of surface wave dispersion curves in weakly laterally varying structures: *Near Surface Geophysics*, 9, 561–570, doi: 10.3997/1873-0604.2011042.
- Boiero, D., 2009, *Surface Wave Analysis for Building Shear Wave Velocity Models*: PhD dissertation, Politecnico di Torino.
- Kennett, B. L. N., 1995, Approximations for surface-wave propagation in laterally varying media: *Geophys. J. Int.*, **122**, 470- 478.
- Marquering, H., R. Snieder, and G. Nolet, 1996, Waveform inversions and the significance of surface-wave mode coupling: *Geophys. J. Int.*, **124**, 258-278.
- Masoni, I., 2016, *Inversion of surface waves in an oil and gas exploration context*: PhD dissertation, Universite Grenoble Alpes.
- McMechan, G.A., and M.J. Yedlin, 1981, Analysis of dispersive wave by wave field transformation: *Geophysics*, 46, 869-874.

- Nazarian, S., and K.H. Stokoe, 1984, in situ shear wave velocity from spectral analysis of surface waves: Proc 8th Conference on Earthquake engineering - St Francisco, vol. 3, Prentice Hall, pp.31-38.
- Neducza, B., 2007, stacking of surface waves: *Geophysics*, 72, no. 2, V51-V58.
- Nolet, G., and G.F. Panza, 1976, Array analysis of seismic surface waves: limits and possibilities: *Pure and Applied geophysics*, 114, 776-790.
- Socco, L. V., and C. Strobbia, 2004, Surface-wave method for near-surface characterization: A tutorial: *Near Surface Geophysics*, 2, 165–185, doi: 10.3997/1873-0604.2004015
- Socco, L. V., S. Foti, and D. Boiero, 2010, Surface-wave analysis for building near surface velocity models — Established approaches and new perspectives: *Geophysics*, 75, no. 5, 75A83–75A102, doi: 10.1190/1.3479491.
- Strobbia, C., 2003, *Surface Wave Method: Acquisition, Processing and Inversion*: PhD dissertation, Politecnico di Torino.
- Tselentis, G.A., and G. Delis, 1998, Rapid assessment of S-wave profiles from the inversion of multichannel surface wave dispersion data: *Annali di Geofisica*, 41, 1-15.
- Woodhouse, J.H., 1974, Surface waves in a laterally varying layered structure: *Geophys. J. R. astr. Soc.*, **37**, 461-490.

Yanovskaya, T.B., 2002, Asymptotic ray theory for seismic surface waves in laterally inhomogeneous media, *Stud. geophys. geod.*, **46**, 267-282.